Human Molecular Genetics, 2020, Vol. 29, No. 19 3266–3284

doi: 10.1093/hmg/ddaa202
Advance Access Publication Date: 24 September 2020
General Article

GENERAL ARTICLE

A novel mouse model for pyridoxine-dependent epilepsy due to antiquitin deficiency

Hilal H. Al-Shekaili[1], Terri L. Petkau[2], Izabella Pena[3], Tess C. Lengyell[2], Nanda M. Verhoeven-Duif[4], Jolita Ciapaite[4], Marjolein Bosma[4], Martijn van Faassen [5], Ido P. Kema[5], Gabriella Horvath[6], Colin Ross[7], Elizabeth M. Simpson[1,2], Jan M. Friedman[1,8], Clara van Karnebeek[9,10,11] and Blair R. Leavitt[2,*]

[1]British Columbia Children's Hospital Research Institute, Department of Medical Genetics, University of British Columbia, Vancouver, BC, Canada, [2]Centre for Molecular Medicine and Therapeutics, BC Children's Hospital Research Institute, Department of Medical Genetics, University of British Columbia, Vancouver, BC, Canada, [3] Whitehead Institute for Biomedical Research, Cambridge, MA 02142, USA, [4]Department of Genetics, University Medical Center, Utrecht, The Netherlands, [5]Department of Laboratory Medicine, University Medical Center Groningen, University of Groningen, Groningen, The Netherlands, [6]Division of Biochemical Diseases, Department of Pediatrics, University of British Columbia and BC Children's Hospital, Vancouver, BC, Canada, [7]Faculty of Pharmaceutical Sciences, University of British Columbia, Vancouver, BC, Canada, [8]Department of Medical Genetics, University of British Columbia, Vancouver, BC, Canada, [9]Department of Pediatrics, Centre for Molecular Medicine and Therapeutics, BC Children's Research Institute, University of British Columbia, Vancouver, BC, Canada, [10]Department of Pediatrics, Emma Children's Hospital, Amsterdam University Medical Centres, Amsterdam, The Netherlands and [11]Department of Pediatrics, Amalia Children's Hospital, Radboud University Medical Centre, Nijmegen, The Netherlands

*To whom correspondence should be addressed at: Centre for Molecular Medicine and Therapeutics (CMMT), The University of British Columbia and BC Children's Hospital, Room 2020, 950 West 28th Ave, Vancouver, BC V5Z 4H4, Canada. Tel: +1 604 875 3801; Fax: +1 604 875 3840; Email: bleavitt@cmmt.ubc.ca

Abstract

Pyridoxine-dependent epilepsy (PDE) is a rare autosomal recessive disease caused by mutations in the *ALDH7A1* gene leading to blockade of the lysine catabolism pathway. PDE is characterized by recurrent seizures that are resistant to conventional anticonvulsant treatment but are well-controlled by pyridoxine (PN). Most PDE patients also suffer from neurodevelopmental deficits despite adequate seizure control with PN. To investigate potential pathophysiological mechanisms associated with *ALDH7A1* deficiency, we generated a transgenic mouse strain with constitutive genetic ablation of *Aldh7a1*. We undertook extensive biochemical characterization of *Aldh7a1*-KO mice consuming a low lysine/high PN diet. Results showed that KO mice accumulated high concentrations of upstream lysine metabolites including Δ^1-piperideine-6-carboxylic acid (P6C), α-aminoadipic semialdehyde (α-AASA) and pipecolic acid both in brain and liver tissues, similar to the biochemical picture in *ALDH7A1*-deficient patients. We also observed preliminary evidence of a widely

Received: April 23, 2020. **Revised:** August 18, 2020. **Accepted:** August 27, 2020

deranged amino acid profile and increased levels of methionine sulfoxide, an oxidative stress biomarker, in the brains of KO mice, suggesting that increased oxidative stress may be a novel pathobiochemical mechanism in *ALDH7A1* deficiency. KO mice lacked epileptic seizures when fed a low lysine/high PN diet. Switching mice to a high lysine/low PN diet led to vigorous seizures and a quick death in KO mice. Treatment with PN controlled seizures and improved survival of high-lysine/low PN fed KO mice. This study expands the spectrum of biochemical abnormalities that may be associated with *ALDH7A1* deficiency and provides a proof-of-concept for the utility of the model to study PDE pathophysiology and to test new therapeutics.

Introduction

Pyridoxine-dependent epilepsy (PDE, Phenotype MIM # 266100) is a rare autosomal recessive disease with incidence estimates that average 1:64,352 over different subpopulations (1). PDE is characterized by recurrent perinatal-onset seizures that are resistant to conventional anticonvulsant treatment but show remarkable response to the administration of pyridoxine (PN). Seizures usually relapse when PN treatment is discontinued either incidentally or for diagnostic purposes. Most PDE patients also exhibit developmental delay and moderate to severe intellectual disability along with, in some cases, structural brain abnormalities (2), most commonly hypoplasia of the corpus callosum and/or cerebellum (3, 4). The phenotypic spectrum may also include non-neuronal features like ocular problems, hypoglycemia, hypothyroidism, profound electrolyte disturbances and diabetes insipidus (2, 5, 6).

PDE is caused by homozygous or compound heterozygous mutations in the *ALDH7A1* gene (antiquitin, ATQ) and consequent loss of activity of α-aminoadipic semialdehyde dehydrogenase, an enzyme that functions within the lysine catabolism pathway (3). Loss of this enzyme's function in turn leads to the accumulation of three intermediate lysine catabolites: Δ^1-piperideine-6-carboxylic acid (P6C), α-aminoadipic semialdehyde (α-AASA) and pipecolic acid (PIP) (2) (Fig. 1). Deficiency of ALDH7A1 is thought to cause seizures because accumulating P6C condenses with PLP and inactivates this cofactor that is essential for neurotransmitter metabolism (3).

About 70% of PDE patients suffer intellectual disability and/or developmental delay even with early PN treatment and adequate seizure control (7). Despite discovery of *ALDH7A1* deficiency as a genetic cause of PDE in 2006, the pathophysiological mechanisms underlying the observed brain structural abnormalities and neurodevelopmental impairments have remained incompletely understood. Progress in this field has been hampered by two factors: difficulty in studying biochemical and neuropathological changes directly in patients' tissues and the lack of an appropriate animal model for PDE. In 2017, the first vertebrate model of antiquitin deficiency was developed and characterized (8). Zebrafish deficient for the *aldh7a1* gene display biochemical and behavioral phenotypes that closely mimic human PDE patients. While useful for investigating disease pathogenesis and potential drug screening, a mouse model of antiquitin deficiency would allow further study of disease mechanisms in a mammalian system and is a requirement for pre-clinical therapeutic testing.

Devising effective treatments to prevent the neurodevelopmental disorder in PDE patients has been challenging. Dietary lysine restriction along with arginine supplementation—termed triple therapy in combination with PN—has recently been shown to improve neurodevelopmental outcomes if introduced early in life (9). However, this therapy is not effective in all patients, can be demanding in terms of compliance, and is sometimes associated with side effects (10, 11).

ALDH7A1 deficiency is thought to cause two concomitant abnormalities in PDE; accumulation of upstream metabolites and depletion of intracellular PLP (5). It has been proposed that cellular injury might be caused by build-up of lysine catabolites in the brain (12), which do not normalize on conventional PN therapy. Available data on brain concentrations of these neurotoxic compounds, mainly P6C and α-AASA, are limited to a single post-mortem study in a PDE patient (12). Depletion of intracellular PLP is speculated to occur based on biochemical experiments but has not been demonstrated in patients. The current state of knowledge does not provide a mechanistic link between *ALDH7A1* deficiency and the extra-neuronal abnormalities seen in PDE patients.

In an important milestone towards filling these knowledge gaps in disease biology and to produce a platform for therapeutic trials, we report the development of a novel mouse model for PDE by targeted ablation of *Aldh7a1* in embryonic stem cells. The report includes the results of biochemical characterization of *Aldh7a1*-null mice under a low lysine/high PN diet along with seizure and survival analyses on lysine and PN-modified diets. We tested the mice for the presence of the two main biomarkers in PDE patients, P6C and α-AASA. We additionally explored various other metabolic compounds for abnormal profiles that might be indirectly caused by the enzymatic defect. The data provide the first proof-of-concept for the disease model, including a metabolic signature consistent with blockade of the lysine catabolism pathway in *Aldh7a1*-deficient mice and a diet-induced, PN-responsive clinical seizure phenotype.

Results

Establishing *Aldh7a1*-targeted strains

We generated three *Aldh7a1*-targeted strains of mice by blastocyst injection of ESC's carrying the *Aldh7a1*$^{tm1a(EUCOMM)Hmgu}$ allele followed by sequential crossings with mice ubiquitously expressing Cre recombinase or FLPo recombinase, respectively: reporter-tagged (tm1b allele), conditional floxed (tm1c allele) and constitutive KO (tm1d allele) mice (Fig. 2A). Mice were maintained on our facility's standard chow (referred to as 'regular' diet hereafter in reference to its standard facility use and independent of nutrient content), which contains 0.9% lysine and 18 ppm PN. We note this up front as diet is subsequently shown to have a significant effect on the phenotype of this mouse model (Figs 6–8).

Intercrossing heterozygous KO (HET) mice resulted in live homozygous KO (KO) offspring that were able to reach adulthood. However, based on genotyping done at weaning, KO mice occurred with significantly lower than expected frequency

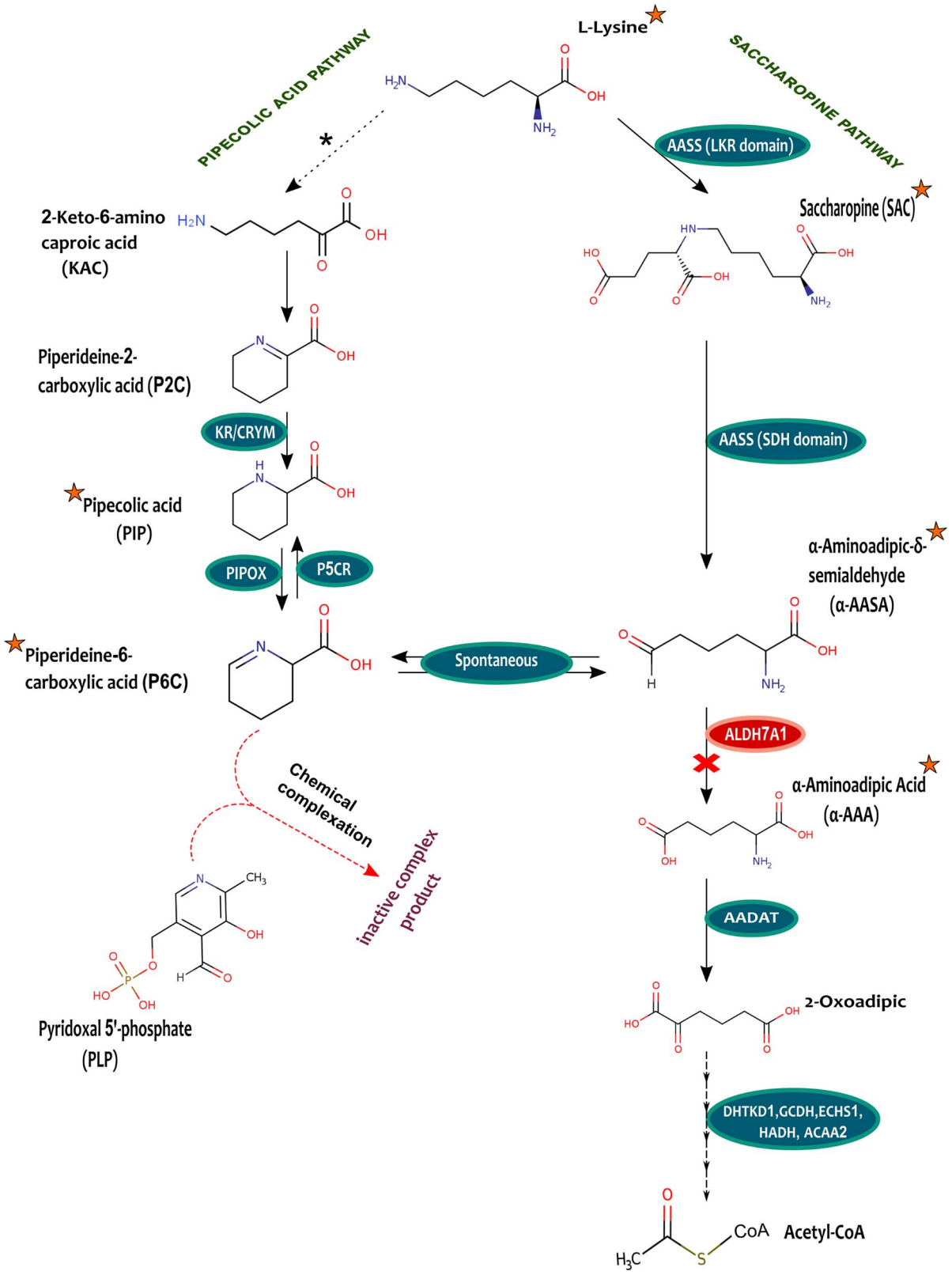

Figure 1. Pipecolic acid (left) and saccharopine (right) pathways for L-lysine catabolism in mammals. ALDH7A1 catalyzes the step indicated by the red 'X.' Inactivation of the enzyme in PDE causes buildup of its two substrates: P6C and α-AASA. Through Knoevenagel condensation, accumulating P6C complexes with PLP forming an inactive adduct and leading to depletion of the cofactor. Colored star symbols denote the compounds that were analyzed in *Aldh7a1*-KO mice. * The nature of the first step of pipecolic acid pathway has remained undetermined. AASS: aminoadipic semialdehyde synthase, LKR: lysine-ketoglutarate reductase, SDH: saccharopine dehydrogenase, AADAT: 2-aminoadipate aminotransferase, KR: ketimine reductase, PIPOX: pipecolic acid oxidase, P5CR: piperideine-5-carboxilic reductase (based on Pena *et al.* (18) and Hallen et al. (26)).

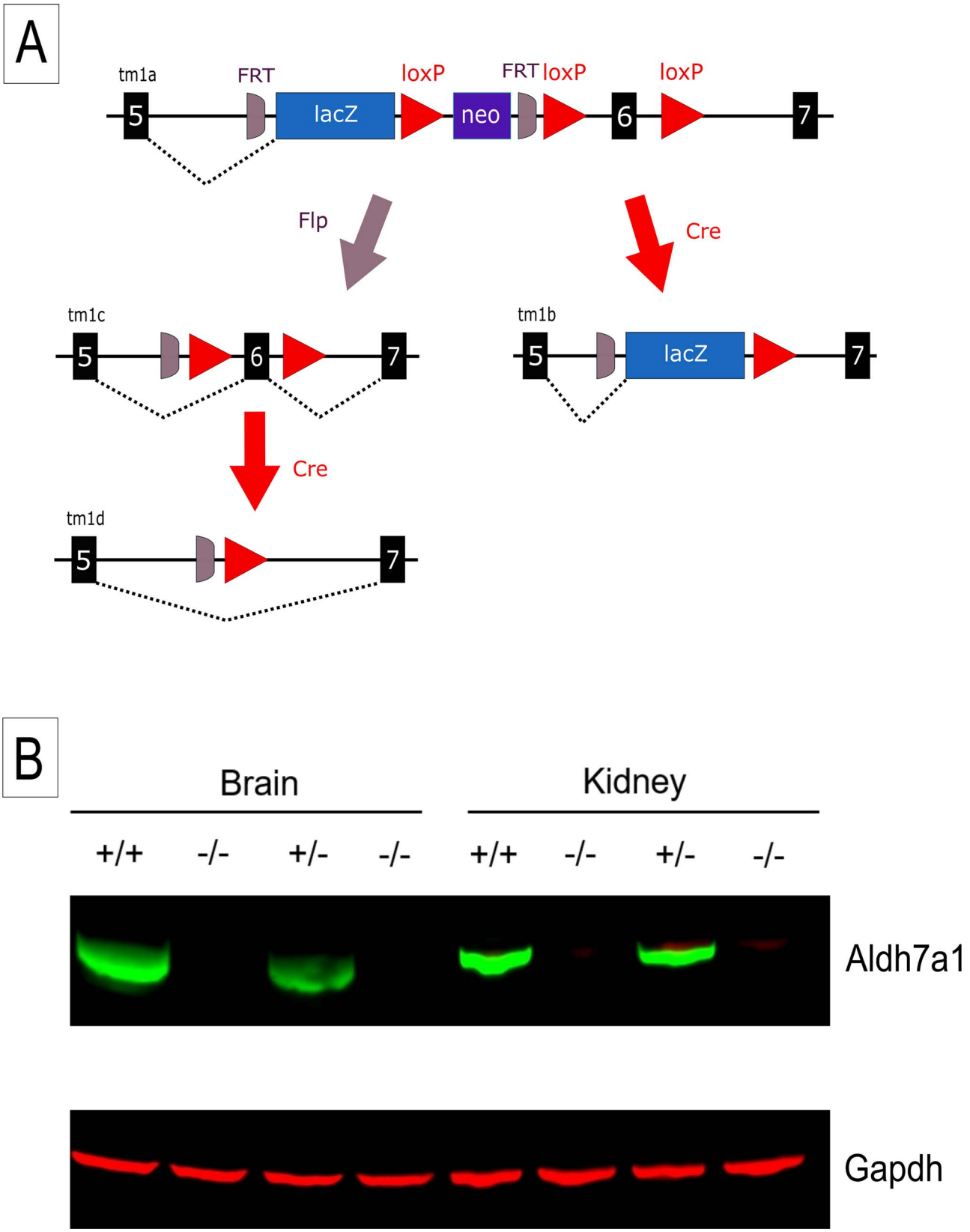

Figure 2. Generation of *Aldh7a1*-targeted mice. (**A**) Flowchart showing targeting strategy, breeding scheme used to generate each strain and structure of different mutant alleles: tm1a (full inserted construct), tm1b (lacZ-tagged), tm1c (conditional) and tm1d (deletion). Numbered boxes represent *Aldh71* exons. (**B**) Western immunoblot from brain & kidney homogenates showing complete absence of Aldh7a1 expression in the homozygous KO (−/−) as compared with WT (+/+) and heterozygous KO (+/−) mice. Gapdh (red) was used as a loading control.

(Supplementary Data, Table S1). Adult KO mice were indistinguishable from their WT littermates in size, appearance and apparent home cage behavior. No spontaneous seizure activity was noted on short-term visual inspection of KO mice. Western blot analysis of brain and kidney homogenates confirmed complete loss of Aldh7a1 expression in KO mice (Fig. 2B).

Analysis of lysine metabolites

To gain insight into the metabolic consequences of *ALDH7A1* deficiency, we quantified multiple metabolic intermediates surrounding the ALDH7A1-catalyzed step in the lysine catabolism pathway in brain and liver tissues of heterozygous and homozygous KO mice versus their WT counterparts. In adult mice, three upstream lysine catabolic products (P6C, α-AASA and PIP) accumulated in significantly higher concentrations in brain and liver tissues of KO mice compared with low or undetectable levels in HET and WT mice (Fig. 3A). Lysine, on the other hand, had a significantly lower concentration in the brains of adult KO mice (Supplementary Data, Fig. S1). In P0 mice, a slightly different set of lysine catabolites were measured (see Methods for explanation). All assayed lysine catabolites (P6C, PIP, SAC and α-AAA) were present in significantly higher concentrations in the brain tissue of KO mice (Fig. 3B and Supplementary Data, Fig. S1). In liver tissue from P0 mice, PIP was significantly elevated in KO mice compared with WT mice (Fig. 3B). P6C and SAC tended to be higher in the liver of P0 KO mice compared with WT (Fig. 3B). Thus, *Aldh7a1*-null mice display biochemical abnormalities that closely recapitulate those seen in PDE patients with *ALDH7A1* mutations.

Longitudinal analysis of P6C and PIP levels showed that, on average, P6C accumulated to higher levels in brain tissue from adult KO mice compared with that of neonatal mice (156.1 ± 12.48 versus 66.05 ± 9.856 nmol/g, mean $\pm$ SEM, $P = 0.0004$), while a converse trend was observed for PIP (395.8 ± 32.96 nmol/g in P0 versus 205.4 ± 21.74 nmol/g in adults, mean $\pm$ SEM, $P = 0.0004$) (Supplementary Data, Fig. S2). Tissue-specific differences were also observed. P6C was present at a nominally higher average concentration in liver tissue compared with brain in adult KO mice (210.6 ± 25.64 versus 156.1 ± 12.48 nmol/g, mean $\pm$ SEM, $P = 0.0763$). PIP, on the other hand, accumulated to significantly higher levels in brain versus liver tissue in both neonatal and adult KO mice (neonatal: 395.8 ± 32.96 versus 109.2 ± 39.88 nmol/g, mean $\pm$ SEM, $P = 0.0005$; adult: 0.2054 ± 0.02174 versus 0.08763 ± 0.007993, nmol/g, mean $\pm$ SEM, $P = 0.0002$) (Supplementary Data, Fig. S3). As noted previously in patients (13), the levels of P6C and its open-chain isomer, α-AASA, correlated significantly in all tested tissues ($R^2 = 0.9301$, $P < 0.0001$) (Supplementary Data, Fig. S4). Taken together, the data indicate robust dysregulation of lysine metabolites in *Aldh7a1*-null mice.

Analysis of vitamin B6 vitamers and amino acids

A comprehensive battery of vitamin B6 (vitB) vitamers (pyridoxine (PN), pyridoxal (PL), pyridoxamine (PM) and their phosphorylated forms: PNP, PLP and PMP, respectively), along with their major catabolite, 4-pyridoxic acid (PA), were analyzed in the plasma, brain and liver of adult mice. As increased P6C is thought to deplete PLP levels in PDE patients, we hypothesized that this vitamer would be lower in KO mice compared with WT mice. Results, however, demonstrated no significant difference in the concentration of vitB6 vitamers between KO and WT adult animals in tested tissues and fluids under the current experimental paradigm (Fig. 3 and Supplementary Data, Fig. S5B). VitB6 vitamers were also analyzed in brain tissue from P0 animals. There were no significant differences in levels of PLP, PL and PMP between WT and KO P0 mice (Supplementary Data, Fig. S5A); all other vitamers assayed (PNP, PN, PM) and PA were below the level of detection for both genotypes.

A panel of 22 amino acids was analyzed in brain and liver tissues of adult mice using targeted ultra-performance liquid chromatography–tandem mass spectrometry (UPLC–MS/MS) methods to explore potential amino acid dysregulation. Measurements showed a number of abnormal amino acid profiles in brain and liver of KO mice. In brain, glycine was present at significantly lower levels compared with WT mice while ornithine was elevated (Fig. 4A). In liver, the effect was more pronounced where 11 amino acids had abnormally elevated levels in KO mice (Fig. 4B).

Finally, we quantified the levels of methionine sulfoxide, an oxidative stress biomarker, in brain (Fig. 5A) and liver (Fig. 5B) tissues. Methionine sulfoxide showed elevated concentrations in brain tissue of HETs and KOs relative to WT mice (Fig. 5A). Thus, *Aldh7a1*-null mice display specific alterations in some amino acids and an oxidative stress marker, indicating the presence of underlying biochemical abnormalities.

Analysis of neurotransmitters

As another exploratory study, we examined KO mice for abnormalities in a set of neurotransmitters. Gamma-aminobutyric acid (GABA) and glutamic acid were assayed in neonatal and adult brain and liver tissue. Results showed no significant differences in the levels of these neurotransmitters between the three genotypes (Supplementary Data, Fig. S6).

Further analysis included a more comprehensive panel of 10 monoamine neurotransmitters and/or their metabolites (L-DOPA, dopamine, epinephrine, norepinephrine, 3-methoxytyramine, normetanephrine, metanephrine, 5-hydroxytryptophan [5-HTP], serotonin and 5-hydroxyindoleacetic acid [5-HIAA]) in brain and plasma of adult mice. Two compounds, norepinephrine and its metabolite, normetanephrine, were present at significantly higher concentrations in the plasma of KO mice compared with WTs (Fig. 5C and D, Supplementary Data, Fig. S7 for remaining neurotransmitters). Overall, large scale differences in neurotransmitters in the brain were not observed in *Aldh7a1*-null mice, but specific changes in two plasma metabolites suggest additional underlying biochemical abnormalities that result from antiquitin deficiency.

In vivo electrophysiology

A total of 48–96 h of multi-channel EEG recordings were obtained from 3 WT and 3 KO mice of mixed sex at 10 months of age on the regular diet. There was no evidence of convulsive seizures in KO mice consuming this diet by analysis of these EEG data.

Behavioral and neuropathological analysis

A battery of behavioral tests was conducted on *Aldh7a1*-KO mice at two time points: 2.5 and 6 months. These tests were used to assess locomotor activity (open field), anxiety-like behavior (open field, elevated plus maze and novel object recognition), depressive-like behavior (forced swim test), spatial memory and learning (Morris water maze), and motor coordination and motor learning (accelerating rotarod). Analysis of the results using standard pipelines revealed no differences

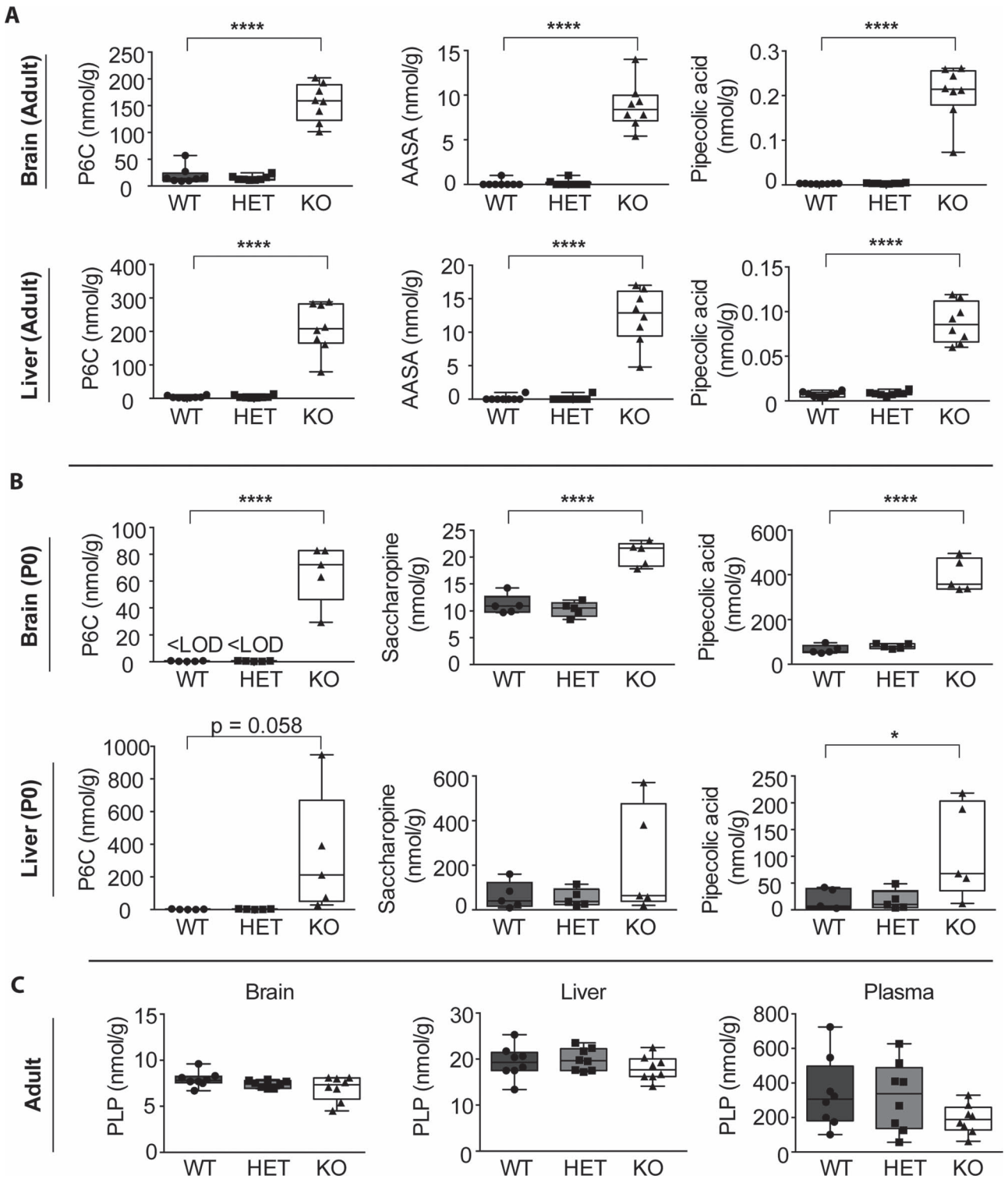

Figure 3. *Aldh7a1*-null mice reproduce the human biochemical phenotype of PDE patients. (**A**) Mass spectrometry data from brain (upper) and liver (lower) of adult mice showing elevated levels of the three key biomarkers in PDE in homozygous KO (KO) mice compared with low or no detectable levels in wildtype (WT) and heterozygous KO (HET) mice. (Boxes extend from 25th to 75th percentiles, horizontal lines inside boxes represent median values, whiskers extend from min to max values.) (****$P < 0.0001$). (**B**) Mass spectrometry data from brain (upper) and liver (lower) of P0 mice showing accumulation of lysine metabolites, P6C, pipecolic acid and saccharopine in homozygous KO mice (KO) (LOD: limit of detection) (*$P < 0.05$, ****$P < 0.0001$ by one-way ANOVA followed by Dunnett's *post-hoc* test). (**C**) Mass spectrometry data from adult mice on regular diet showing no significant differences in PLP levels between the 3 genotypes.

in performance between WT and KO mice at either age analyzed (Supplementary Data, Figs S8 and S9).

We performed qualitative assessment of neuropathological changes in *Aldh7a1-KO* mice at 4 months of age using immunohistochemical staining with NeuN and GFAP. Coronal serial brain sections from WT and KO mice were examined for gross structural differences, neuronal distribution, neuronal density and the presence of astrogliosis in multiple brain

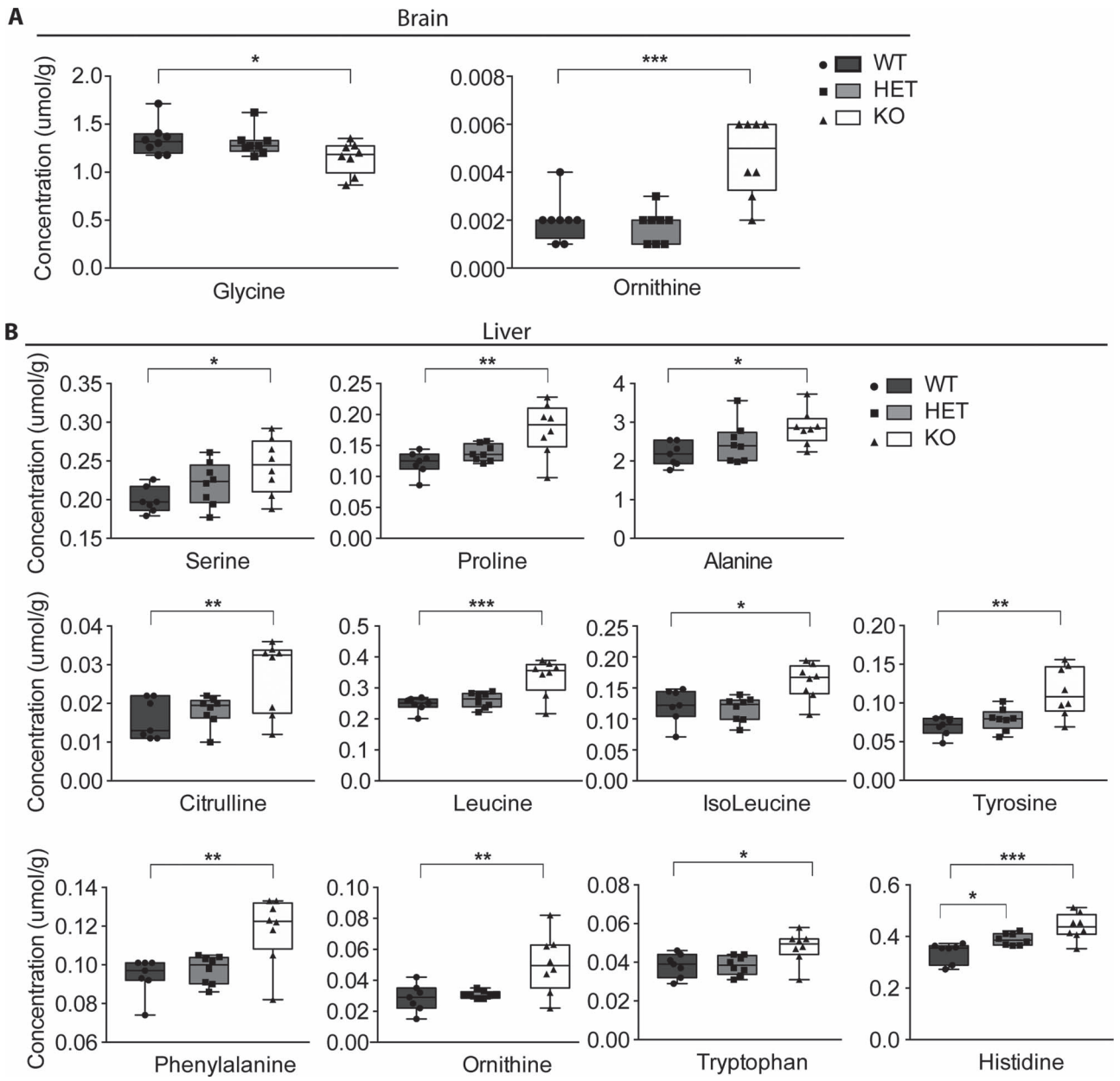

Figure 4. Quantification of amino acid levels in *Aldh7a1*-deficient mice reveals multiple abnormalities. (**A**) Amino acid quantification in adult brain shows significant changes in 2 amino acids (*$P < 0.05$, ***$P < 0.001$). (**B**) Amino acid quantification in adult liver reveals aberrant profile across 11 amino acids (*$P < 0.05$, **$P < 0.01$, ***$P < 0.001$ by one-way ANOVA followed by Dunnett's *post-hoc* test).

regions. No differences were apparent between WT and KO mice in the assessed neuropathological features (Supplementary Data, Fig. S11). There were also no differences between the two genotypes in brain weight measured at either 2.5 or 6 months of age (2.5 months: WT 352 ± 3 mg; KO 388 ± 10 mg. 6 months: WT 398 ± 4 mg; KO 386 ± 6 mg). Thus, despite a clear demonstration of metabolite changes, no cognitive or neuropathological abnormalities were observed in KO mice under this experimental paradigm.

Dietary induction trials

Hypothesizing that dietary manipulation of lysine and/or PN levels might affect seizure susceptibility in KO mice, we conducted a pilot trial to determine the response of KO mice to a diet with high (4.7%) lysine content and low (1.6 ppm) PN (SD1). To exclude strain-specific effects, and given that the C57BL/6 J (B6/J) strain is known to be relatively seizure-resistant (14–17) and that our own empirical experience has shown that seizure susceptibility can be highly variable on this background, we chose to include a KO mouse incipient congenic on the 129 S1/SvImJ (129) background in this experiment. A single B6/J KO mouse and a 129 KO mouse fed SD1 both died 36–48 h from the start of the diet due to uncontrolled seizures as was evident from analysis of their EEG recordings. Clinical seizures were visually noted in the B6/J mouse as early as 23.5 h post-diet (PD) administration, at which point the mouse had consumed 2.63 g of the diet. Analysis of a continuous 17-h EEG recording from this mouse revealed the presence of recurrent epileptiform discharges. The discharges, which were

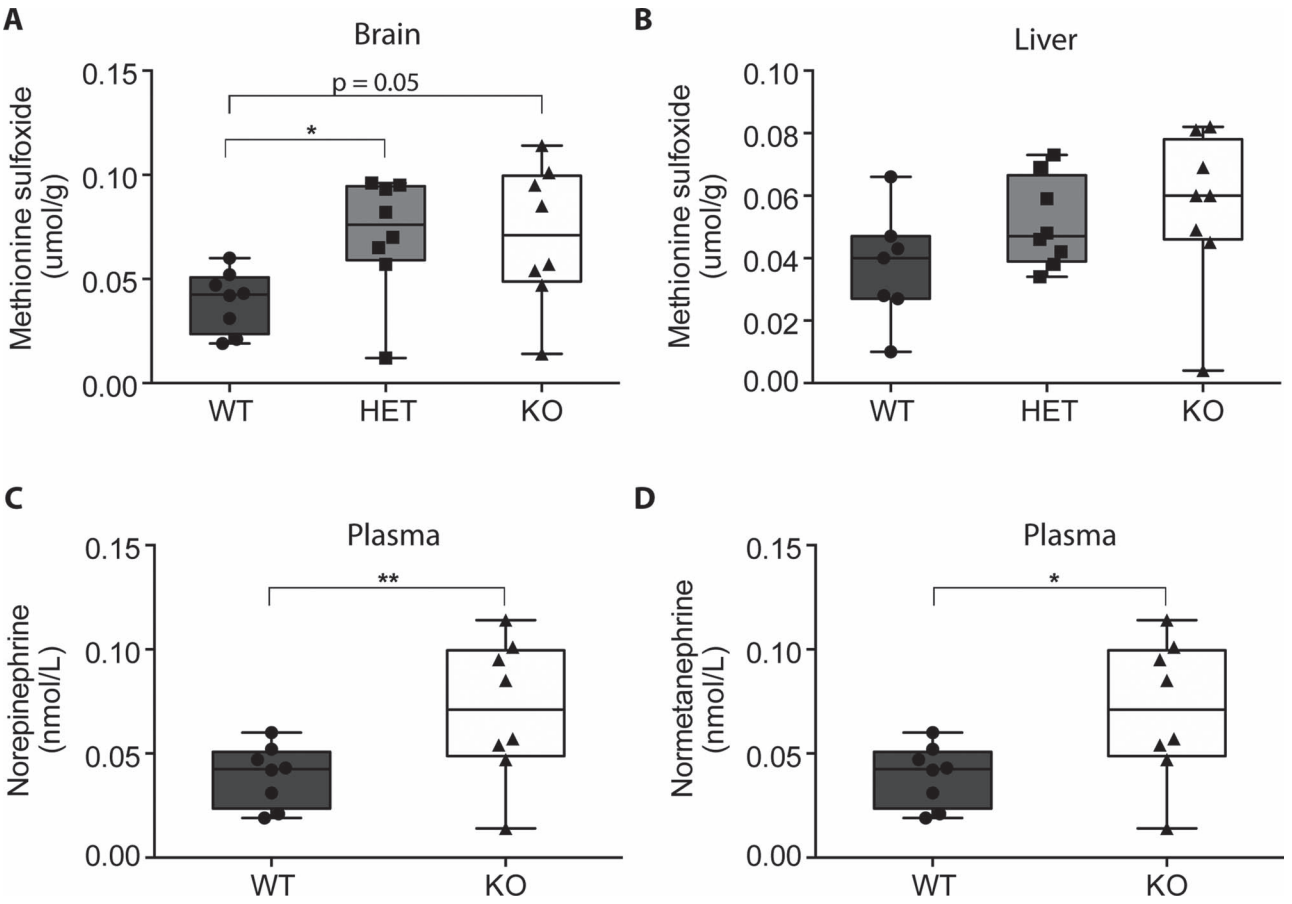

Figure 5. Novel biochemical changes are present in *Aldh7a1*-deficienct mice. Top: Measurement of oxidative stress biomarker, methionine sulfoxide, in brain (A) and liver (B) of adult mice uncovers high levels in brain of KO (borderline significant) and HET mice (*$P < 0.05$). Bottom: Graphical representation of LC–MS/MS analysis of norepinephrine (C) and its metabolite, normetanephrine (D), in plasma of KO versus WT mic (*$P < 0.05$, **$P < 0.01$ by one-way ANOVA followed by Dunnett's *post-hoc* test).

synchronous in all EEG channels, correlated with abrupt and intense movement changes along the three accelerometer axes, indicative of a convulsive seizure (Fig. 6). Typical EEGs during the ictal discharges are shown in Fig. 6. In the 129 mouse, a total of 46.9 h of continuous EEG recording was collected. Analysis showed frequent electroclinical seizure events with the first seizure occurring 31.9 h PD. Multiple electrographic patterns were noted including focal, generalized and burst-suppression (Supplementary Data, Fig. S8). Supplementary Data, Figure S9 shows an example of ictal EEG during generalized seizures in this mouse. Epileptiform discharges seemed to become progressively worse with time, initially emerging as isolated single spikes followed by poly-spikes without a clinical correlate, then focal followed by severe generalized seizures and culminating in burst-suppression status epilepticus (SE). Burst-suppression was also the dominating terminal seizure pattern in the B6/J mouse (Fig. 7). Post- and inter-ictal spikes were also frequently observed in both mice (Fig. 6 & Supplementary Data, Figs S9 and S10) and seizures were occasionally followed by long periods of post-ictal behavioral arrest (freezing). Both mice had a prolonged SE (lasting for up to 29 min) in the form burst-suppression prior to death. The amount of diet each mouse had consumed until death was 2.77 g for the B6/J mouse and 2.95 g for the 129 mouse. All other mice (WTs and PN-treated KOs) survived to the end of study. Analysis of EEG data collected from two PN-treated KOs under SD2 (54.25 h) and two WT under SD1 (93 h) showed no epileptic seizures. Reducing the PN dose to 100 µg/g q.d. and postponing one dose by 12 h did not cause any seizure activity. It was therefore empirically determined that a dose of 200 µg/g given every other day (q.o.d.) should be sufficient to prevent seizures. This new PN regimen was implemented in the follow-up trial described below.

A subsequent follow-up trial was conducted in which four B6/J KO mice received SD1. All four of these mice exhibited seizures. Based on visual monitoring, seizure onset in the first three mice ranged from 24.25 to 26.5 h PD while in the fourth mouse the first noted seizure was at 47.2 h PD. Following the first seizure, mice had multiple episodes of severe SE lasting for 3–13 min, which reached the humane endpoint, and were subsequently euthanized at 27.4–51.3 h PD. By the time they were euthanized, the mice had consumed 1.82–3.41 g of diet. No seizures were noted in WT and PN-treated KO mice. One PN-treated KO mouse under SD2 was excluded from the study because of non-compliance with the diet. All other mice survived to the end of the study. Their total diet consumption by the end of the study ranged from 8.01 to 16.39 g in PN-treated KO mice and from 15.73 to 21.0 g in WT mice. Follow-up dietary trials were terminated on Day 10. Figure 8 shows a comparison of survival curves between mice under different tested diets and PN treatment ($P < 0.0001$).

Finally, we sought to confirm that KO mice develop PN-dependent seizures due to the depletion of PLP as a result of

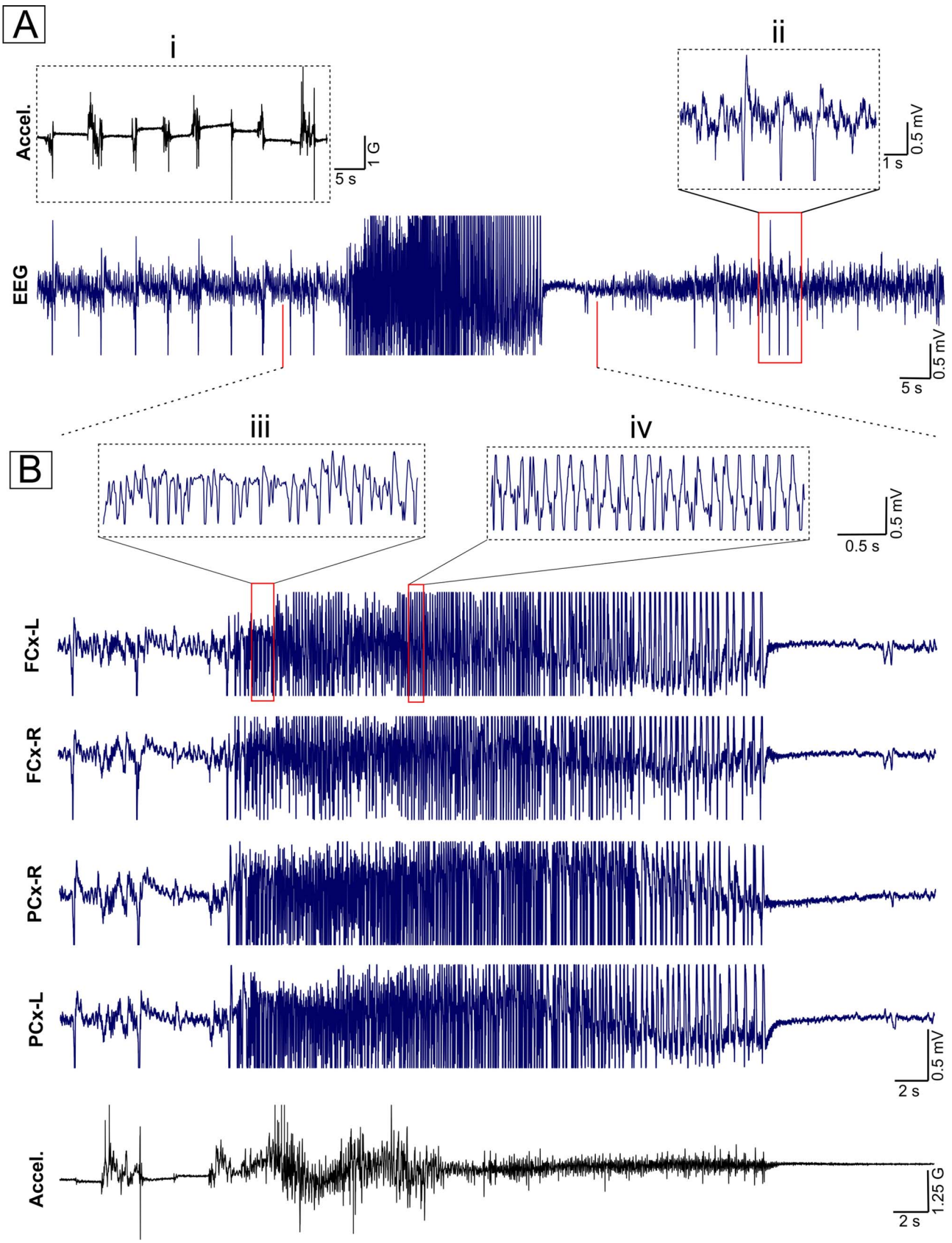

Figure 6. Representative EEG from untreated KO mouse (B6/J strain) under SD1 showing epileptiform discharges. (**A**) Condensed view of 150-s epoch showing a burst of high-amplitude discharges. (**B**) Expanded views of the burst showing synchronous ictal discharges from the four EEG channels along with concurrent trace from accelerometer x-axis. The onset of the discharges coincides with changes in the accelerometer that becomes more intense with time and then tapers down and flattens

disruption to the lysine metabolism pathway. Analysis of PLP levels showed that KO mice consuming SD1 had significantly lower PLP in the brain (Fig. 8B) and the liver (Fig. 8C) compared with WT mice consuming SD1, while PN treatment of KO mice restored PLP to levels near that of WT (Fig. 8B and C). Thus, KO mice develop robust seizures that lead to death but can be controlled by administration of PN, which accurately replicates PDE due to *ALDH7A1* mutations in human patients.

Discussion

The current work describes the generation, biochemical characterization and seizure susceptibility of a novel mouse model for PDE caused by inactivating mutations in *Aldh7a1*. We found that *Aldh7a1*-KO mice recapitulated many biochemical abnormalities characteristic of PDE patients, suggesting that these mice represent an accurate mouse model of the human disease and will be useful for future therapeutic testing. The discovery of putative novel biochemical changes in KO mice suggests that this mouse model may be useful for uncovering yet unidentified pathophysiological mechanisms contributing to the spectrum of phenotypic abnormalities present in PDE patients. The robust biochemical phenotype and dietary-inducible seizure susceptibility in these mice suggest that they will be a useful tool for studying how intellectual disability and other neurodevelopmental phenotypes occur in PDE patients despite adequate seizure control.

A key observation from our study is that the phenotype of *Aldh7a1*-KO mice is intricately linked to diet. KO mice displayed an array of biochemical changes when consuming our facility's regular chow, which is in fact a diet that is relatively low in lysine and high in pyridoxine. Despite the accumulation of upstream metabolites and an altered amino acid profile, mice on this diet did not show evidence of any cognitive deficits or neuropathological abnormalities, nor did they develop spontaneous seizures. This might be considered a limitation of the model except for the fact that severe, spontaneous seizures and concomitant PLP depletion could be induced by feeding the mice a high lysine/low PN diet. The rapidity with which such a diet was able to induce pyridoxine-sensitive seizures in KO mice suggests that the metabolites that were altered in mice fed regular chow either do not represent toxic species or have not yet accumulated to a toxic level. We postulate that additional biochemical abnormalities will be apparent when KO mice are fed a diet that is higher in lysine than our regular chow, and that this is the most likely explanation for the lack of differences observed in some key metabolites in this study. The strong and fatal seizures observed when KO mice were fed SD1 preclude the ability to assess behavior and confound neuropathological phenotypes, and as such we did not attempt these assessments in mice fed this extreme high-lysine diet. We hypothesize that *Aldh7a1*-knockout (KO) mice will display a cognitive and neuropathological phenotype when fed a diet that is intermediate to regular chow and SD1, and indeed immediate future work will be aimed at testing this hypothesis.

Crossing HET mice yielded KO offspring in a lower ratio compared with the expected Mendelian proportions (19.68% versus expected 25%). This low rate of homozygous KO mice might be suggestive of a partially prenatal or early neonatal lethal phenotype, which is line with recent studies in both an *aldh7a1*-KO zebrafish model (18) and in patients (1). Future work will be aimed at better understanding the exact age at which KO embryos are lost and if there is an associated neuropathological phenotype and/or biochemical profile that can explain this early death.

The primary goal of this study was to establish the biochemical phenotype of *Aldh7a1*-null mice on regular chow. *Aldh7a1*-deficient mice displayed accumulation of supraphysiological levels of the lysine catabolites P6C, α-AASA and PIP, the hallmark biochemical features of PDE (2). In addition to these three known biomarkers, we found that another lysine catabolite, saccharopine (SAC), was also highly elevated in KO mice. A similar observation was reported in the *aldh7a1*-KO zebrafish model by Pena *et al.* (18). This result lends support to previous studies suggesting that the saccharopine pathway is an active lysine catabolism pathway in the brain (8, 19). Evaluation of the more recently established PDE biomarker 6-oxo-pipecolic acid (20) will be included in future studies and may lend additional support to the validity of *Aldh7a1* KO mice as a model of PDE.

Our study reports the level of lysine metabolites in a peripheral tissue, the liver, for the first time in an *in-vivo* model of *Aldh7a1* deficiency. Quantification data revealed that lysine metabolites also accumulate in *Aldh7a1*-null liver at concentrations comparable with or even higher than brain tissue (Fig. 3). The high accumulation of PIP in the liver speaks in favor of an active pipecolic acid pathway in liver as suggested by recent studies (8, 21). Alternatively, it has been proposed that PIP accumulates due to retrograde conversion of saccharopine-derived P6C (22, 23). Given the unidirectional nature of the KR/CRYM reaction (Fig. 1), future analysis of piperideine-2-carboxylic acid (P2C) could serve as a better distinguishing biomarker for the pipecolic acid pathway. Questions remain as to the ultimate fate of accumulated PIP in different tissues, but the accumulation of this metabolite in *Aldh7a1*-null mice suggests that this mouse model may be useful in answering important questions about canonical and non-canonical lysine catabolism.

Interestingly, lysine, the principal pathway substrate, was present in *lower* concentrations in brain tissue of KO mice (Supplementary Data, Fig. S1), which is counterintuitive given the downstream blockade of lysine metabolism. Low plasma lysine levels have been described in a single PDE patient (24). A possible explanation for this phenomenon can be inferred from the study of Crowther *et al.* (2019) who noted an increased activity of the α-aminoadipic semialdehyde synthase (AASS) enzyme in patient-derived *ALDH7A1*-deficient fibroblasts. AASS is a bifunctional enzyme, which catalyzes the first two steps in the saccharopine pathway of lysine catabolism (Fig. 1). AASS's overactivity is expected to increase the lysine degradation rate and hence lowers lysine levels. The notion of AASS upregulation in ALDH7A1 deficiency (19) along with an earlier study showing that the saccharopine pathway is the main stream that fuels the production of cerebral P6C and α-AASA (8) highlight the AASS enzyme as a plausible therapeutic target for PDE.

Unexpectedly, α-AAA, a downstream lysine metabolite, was elevated in the brains of KO mice (Supplementary Data, Fig. S1).

towards the end of the episode. (**C**) Further expanded views showing waveform morphology of post-ictal spikes (ii) and from the beginning (iii) and middle (iv) of the ictal phase. (i): a snapshot of the accelerometer readout in the pre-ictal phase showing brief alterations that concur with pre-ictal spikes. Abbreviations, FCx-L: left frontal cortex, FCx-R: right frontal cortex, PCx-L: left parietal cortex, PCx-R: right parietal cortex, Accel.: accelerometer, sec: seconds, mV: millivolts, G: acceleration of Earth's gravity (~9.8 m/s^2).

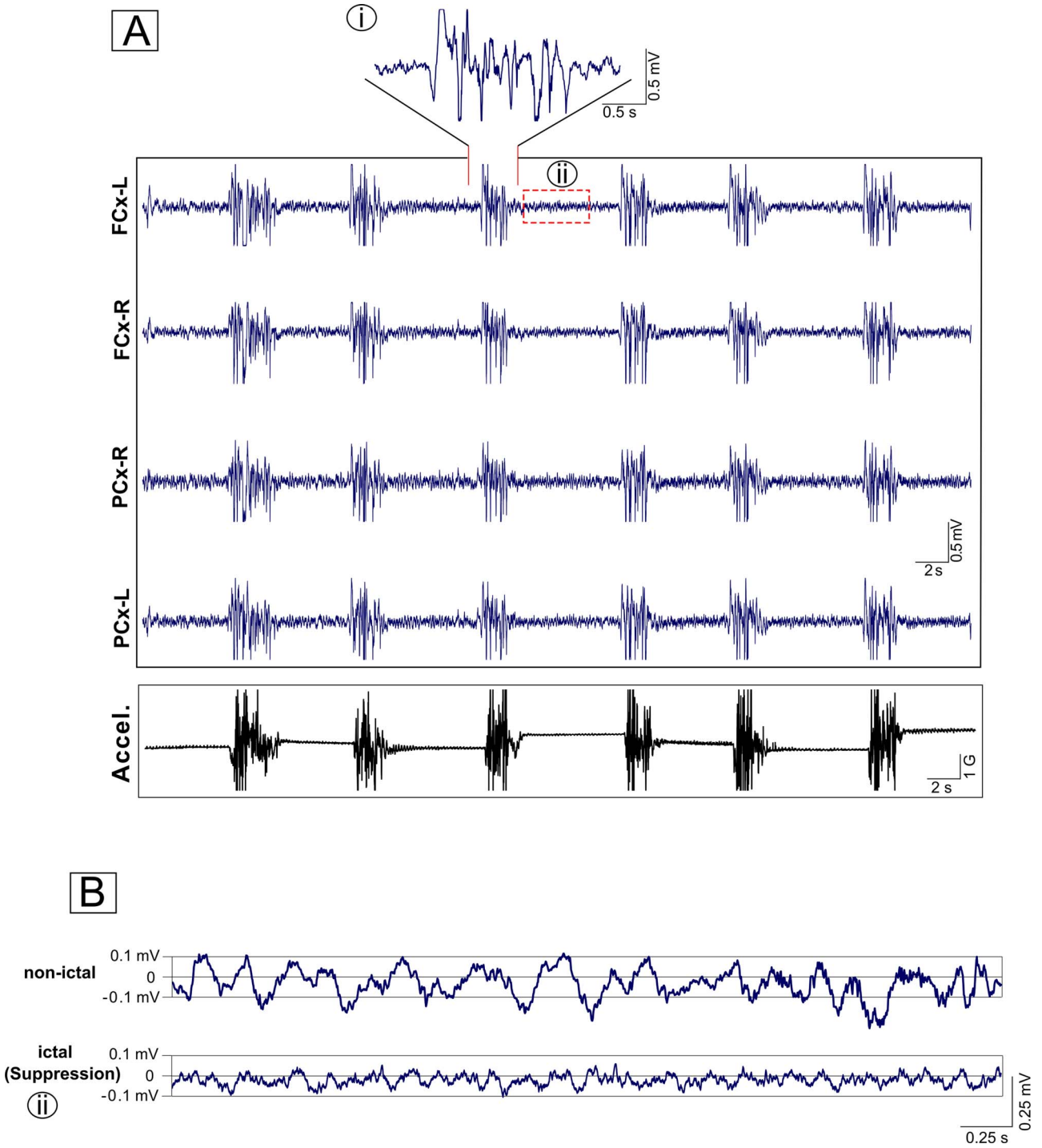

Figure 7. Burst-suppression seizure in untreated KO mouse (B6/J strain) under SD1. (**A**) 4-channel EEG traces showing bursts of polyspikes [expanded in (i)] alternating with periods of suppressed background. Concurrent accelerometer trace shows high-amplitude changes simultaneous with burst episodes on EEG. (**B**) Close-up view of the inter-burst segment delineated by a red box (ii) showing suppressed background compared with normal baseline trace taken form a non-ictal EEG.

In view of the high controversy surrounding a number of steps in the lysine catabolism pathway (8, 19–22, 25–28), our finding may point to the presence in the brain of an alternate route of α-AAA production. We speculate that a new pathway exists that links PIP to α-AAA through yet unknown route which bypasses the ALDH7A1-catalyzed step. A similar hypothesis that re-routes PIP to a further downstream metabolite was put forward by Biagosch *et al.* (2017) in an attempt to explain their unexpected lysine metabolite profile in *Dhtkd1*-/*Gcdh*- double KO mice. The products of both of these genes, *Dhtkd1* and *Gcdh*, function in the lysine catabolism pathway downstream of the metabolic block in ALDH7A1 deficiency. Further investigation using isotopic tracing studies in *Aldh7a1*-deficient mice will help to decipher the origin of accumulating α-AAA in brain.

Comparison of the pattern of lysine metabolites in adult versus P0 KO mice and in brain versus liver revealed a

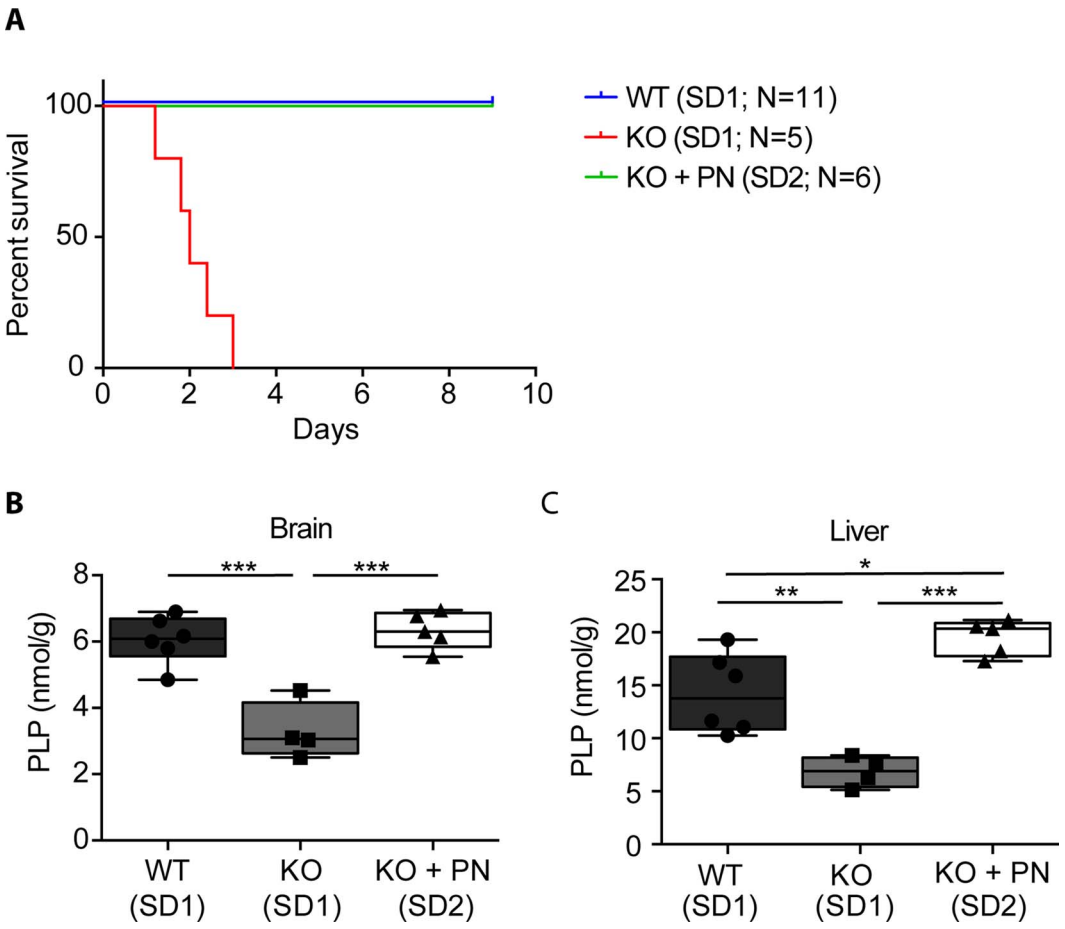

Figure 8. Survival curves comparing mice under modified diets with or without PN treatment. (**A**) High-lysine SD1 induced seizures and acute death in untreated KO mice and PN treatment rescued both phenotypes. Curves are significantly different ($P < 0.0001$). (**B**) PLP concentration in brain and (**C**) in liver after administration of special diets ($^{*}P < 0.05$, $^{**}P < 0.01$, $^{***}P < 0.001$). Abbreviations: KO: *Aldh7a1*-knockout mice; WT: wildtype mice; SD1: special diet 1; SD2: special diet 2.

few noteworthy trends. First, P6C was present in higher concentration in adult compared with neonatal brain (Supplementary Data, Fig. S2A). This may be attributable to less flux through the lysine catabolism pathway during the early neonatal period when active brain development requires the synthesis of more lysine and less is subject to catabolism (9). By further separating adult mice into categories by age in weeks, we observed a trend of escalating concentrations of cerebral P6C with increasing age (Supplementary Data, Fig. S2A). This could indicate that the level of this pathogenic molecule builds up with age, though this cannot be confirmed based on the current data only. A contrary trend to P6C was observed for PIP, which was markedly higher in neonatal than in adult brain (Supplementary Data, Fig. S2B). It was noted that in the developing normal mouse brain, PIP reaches its peak concentration during the perinatal period and then subsides gradually after birth until reaching its lowest levels in adulthood (29). This also correlates with the observation that, in mouse brain, synthesis of PIP from the lysine catabolism pathway occurs at faster rate around birth (26). Tissue-wise in P0 mice, PIP accumulated in higher concentrations in brain compared with liver, while SAC exhibited an opposite trend (Supplementary Data, Fig. S3). These trends could reflect differential activity across the two lysine catabolic pathways between the two organs during the perinatal period, for which there is some support in the developing rat (30). Future experiments evaluating conditionally targeted mice with selective knockdown of *Aldh7a1* in either brain or liver will be useful for teasing apart mechanisms and pathways of lysine metabolism in each of these tissues.

Analysis of amino acids in *Aldh7a1*-deficient mice uncovered several amino acid perturbations (Fig. 4). We note that statistical analysis of amino acids was considered exploratory in this study and results are presented as uncorrected *P*-values; additional studies are required before firm conclusions can be made. Even so, Supplementary Table S2 provides a literature review of the previously reported similar amino acid abnormalities in related human diseases and animal and cellular models. As shown in the table, the majority of amino acid changes observed in this study have also been described in patients with PDE and/or other vitB6-dependent epilepsies. A discrepancy is noted in the glycine profile, which was decreased in the brain of *Aldh7a1*-deficient mice compared with raised levels in CSF of PDE (5) as well as PNPO deficiency patients (31). In concordance with the *Aldh7a1*-deficient mice, low glycine was also reported in vitB6-deprived Neuro-2a cells (32).

Neurotransmitter analysis in *Aldh7a1*-deficient mice was remarkable for elevated norepinephrine and its metabolite, normetanephrine, in plasma (Fig. 5C and D). To our knowledge, neither compound has been previously evaluated in PDE patients. In animal models, high plasma norepinephrine was

observed in pyridoxine-deficient rats (33). Again, confirmatory studies to replicate this finding are required. The possible pathophysiological mechanism underlying the high concentration of this catecholamine in the current model remains unclear.

A more recently discovered cellular function of ALDH7A1 is protection from toxic aldehydes derived from oxidative stress and lipid peroxidation processes (34). In our mouse model, we quantified the levels of methionine sulfoxide, a known and potential biomarker of oxidative stress *in vivo* (35, 36). Quantification data revealed that KO mice accumulated excessive levels of methionine sulfoxide in their brain tissue (Fig. 5A) indicative of increased intracellular ROS content. Interestingly, HET mice had also high cerebral levels of this biomarker which may implicate an indispensable role of ALDH7A1 in cellular detoxification such that even loss of one copy can trigger an oxidative stress abnormality. Additional markers of oxidative stress such as malondialdehyde or 2,3-dinor-8-isoprostane-F2alpha, should be assessed in the future to confirm and/or expand on this finding.

Overall, the data presented here shed light on new possible pathobiochemical mechanisms in ALDH7A1 deficiency. In addition to the previously known metabolites (P6C, α-AASA and PIP), we found accumulation of two other lysine catabolites, SAC and α-AAA. Both of these compounds are reported to cause detrimental cellular effects at high concentrations (37–40). We speculate that the mechanism of neurotoxicity in PDE may additionally involve accumulation of these cytotoxic compounds and reactive aldehyde and oxygen species. In fact, even the cause of metabolic derangements seen in PDE seems be more complex than can be explained by PLP insufficiency alone (26) which is also illustrated, perhaps, by the fact that there was evidence for widely deranged amino acid metabolism in Aldh7a1-deficienct mice despite the lack of a consistent low PLP profile in tested KO mice.

Because of the lack of epileptic phenotype in KO mice under a regular diet coupled with the lack of a clear PLP deficiency at the cellular level, we hypothesized that increasing the amount of dietary lysine would induce seizures in KO mice. To validate this hypothesis, we designed a new diet that is higher in lysine and lower in PN. Testing this diet on KO mice unveiled a vigorous seizure phenotype and led to quick death due to sustained SE. Similarly, in untreated patients, PDE causes prolonged SE that leads to death of affected infants (2, 41, 42). Interestingly, the terminal seizure pattern in these mice was in the form of burst-suppression, a pattern which is also commonly seen in PDE patients (2, 43–45). PN administration abolished seizures in *Aldh7a1*-KO mice, recapitulating the PN responsive seizures in ALDH7A1 deficiency patients and validating our model for PDE. PLP levels were restored to near-normal levels with PN administration (supplemented both in the diet and with peripheral injections), suggesting that PLP plays a causative role in seizure development. Other lysine metabolites in mice fed a high lysine/low PN diet have not been evaluated here, which remains an important future goal in order to determine whether additional factors also play a role in seizure development.

The current study evaluated the biochemical as well as cognitive and neuropathological phenotype of *Aldh7a1*-deficient mice consuming a low-lysine/high PN diet, which is a limitation of the study. First, we note that it was difficult to determine a priori what 'normal' lysine content in the mouse diet is; minimum recommended lysine content is typically determined in terms of growth restriction (46) and is much lower than the lysine content in any commercial diet. On the diet used, some hypothesized differences, such as cognitive impairments and structural changes in the brain, were not observed, while other unexpected phenotypic abnormalities, such as increased levels of α-AAA, and low lysine compared with WT mice, were seen. These observations may indicate that the model does not fully recapitulate the human disease, but further study using diets of varying lysine content is critical before a definitive conclusion can be reached. This is particularly true in light of the reduced PLP observed in mice consuming a high lysine diet (Fig. 8), which clearly demonstrates the dietary dependence of the phenotype in this mouse model. Because of the limited ability to evaluate biochemical changes directly in patients' tissues, it is difficult to determine whether or not the unexpected results that we observed in *Aldh7a1*-deficient mice represent differences between the model and human patients or novel findings regarding lysine metabolism pathways. Most published biochemical investigations in PDE patients have been performed in biofluids (13, 47, 48) or, less commonly, skin fibroblasts (19) which may not reflect the specific changes occurring in brain tissue. Finally, we note that the mice were housed in cages that allowed coprophagia, and this may have contributed to the unexpected levels some metabolites in this study (49). Further investigation of KO mice on varying diets and isotopic tracing studies, combined with evaluating patient-derived samples such as induced pluripotent stem cells, will help to clarify these issues and to discover more about disease biology in the future. Additionally, this study evaluated cohorts of mice of mixed sex but was not powered to determine whether or not there are sex-specific differences in the phenotype of *Aldh7a1*-deficient mice.

In summary, the present report describes the first biochemical and seizure susceptibility data on mice with constitutive genetic ablation of *Aldh7a1*. The data show that the model is amenable to dietary manipulations where, similar to patients, the clinical seizure outcome is dependent on dietary lysine content and PN treatment. The study provides the first insight regarding the metabolite profile in an extracerebral tissue and broadens our knowledge about the spectrum of biochemical abnormalities that may be associated with ALDH7A1 deficiency. It also provides a proof-of-concept for the utility of the model to study PDE pathophysiology and to test new therapeutics that aim to abolish the pathogenic accumulation of metabolites.

Materials and Methods

Generation of constitutive *Aldh7a1* knockout mice

An embryonic stem cell (ESC) line (agouti C57BL/6 N, (50)) with a conditionally targeted allele for *Aldh7a1* (MGI allele name: *Aldh7a1*$^{tm1a(EUCOMM)Hmgu}$) was obtained from the International Knockout Mouse Consortium (IKMC). These genetically modified ESCs harbor a targeting construct that is incorporated between exons 5 and 6 of the *Aldh7a1* gene. The mutant allele with a full version of the targeting construct is known as *tm1a*. As shown in Figure 2A, the tm1a allele contains multiple built-in features that, using different breeding strategies, allows the generation of three strains of mice; lacZ-tagged (tm1b), conditionally targeted or 'floxed' (tm1c) and constitutive null or 'KO' (tm1d) mice. Three clones of the imported ESCs were microinjected into C57BL/6 J blastocysts and implanted in pseudopregnant female mice. Resulting chimeric male mice were backcrossed with wild-type (WT) C57BL/6 J female mice (JAX Stock# 000664) to establish germline transmission. Genotype-confirmed germline mice carrying the tm1a allele were crossed with global Cre recombinase-expressing mice (JAX Stock# 003376) to generate

mice that carry the lacZ-tagged tm1b allele. In parallel, tm1a heterozygous mice were also bred with mice ubiquitously expressing FLPo recombinase (Mutant Mouse Resource & Research Centers -MMRRC- Stock# 032247-UCD). Following excision with FLPo, we generated mice in which *Aldh7a1* is expressed normally but exon 6 of the mouse *Aldh7a1* gene is now flanked by loxP sites (floxed mice). These mice, which harbor the conditional tm1c allele, were crossed with Cre recombinase-expressing mice which yielded mice that carry the tm1d allele. The tm1d allele is the constitutive null or KO allele in which the floxed exon is removed. Removal of this critical exon generates a frameshift in exon 7 that introduces a premature stop codon, and results in the loss of *Aldh7a1* expression. Mice from each of these four different strains (tm1a, tm1c, tm1b and tm1d) were identified using allele-specific PCR-based genotyping assays. The tm1d allele mice were backcrossed for at least five generations onto the C57BL/6 J background prior to generating cohorts for experiments, such that all mice used were incipient congenic on the C57BL/6 J background. The tm1d allele was also backcrossed onto the 129S1/SvImJ background for five generations (incipient congenic at $N = 5$). Incipient congenic 129S1/SvImJ mice were used only for *in vivo* monitoring of seizures under regular diet and after induction with a high lysine diet. Unless otherwise noted, mice used in experiments from all genotypes [WT, heterozygous KO (HET) and homozygous KO (KO)] were generated by intercrossing tm1d heterozygotes. For short-term observance of seizures, KO mice were visually inspected in their home cage for 1 h per day.

Mice of mixed sex and from mixed litters were used for all experiments. Analysis of lysine metabolites, amino acids, vitB6 vitamers and neurotransmitters was done in tissues and biofluids derived from the same mice (for adult mice: $N = 8$ WT, 8 HET and 8 KO mice; for P0 mice: $N = 5$ WT, 5 HET and 5 KO except for vitB6 vitamers, where $N = 3$ WT, 3 HET and 3 KO). Samples from P0 mice were collected at postnatal Day 0 and adult samples were collected from mice at ages that ranged from 10.6 to 22 weeks.

The mouse model described in this report was generated in accordance with guidelines of the Canadian Council on Animal Care and under an approved protocol from the University of British Columbia Animal Care Committee (Animal Protocols # A15-0200, A15-0180, A14-0031 and A18-0117). Mice were housed on ventilated racks in a specific pathogen-free barrier facility with a 12 h light/dark cycle in cages that allowed coprophagia. Mice were group-housed with their littermates to a maximum of five mice per cage and given free access to food and water. Mice were fed the standard chow used at our animal facility (Envigo 2018 Teklad Global 18% protein Rodent Diet) containing (w/w) 18% total protein, 0.9% lysine and 18 ppm PN except where otherwise noted. This standard diet is referred to as the 'regular' diet throughout the manuscript based on its standard use in our facility and does not refer to it containing a 'standard' amount of lysine or PN. Published guidelines for minimum nutrient content in rodent diets are based on growth restriction (46) and commercial rodent chows typically contain lysine at a level much higher than this minimum. 'Regular' chow is noted to be low in lysine and high in PN relative to the special diets used for seizure induction.

Western immunoblots

For western immunoblotting, brain and kidney tissue samples harvested from P0 mice killed by decapitation were snap frozen in isopentane. Frozen samples were homogenized in radioimmunoprecipitation assay buffer containing protease inhibitors. About 50 µg of protein from each sample was separated by 12% Bis-Tris gel electrophoresis (Nupage, Invitrogen) and transferred overnight at 30 V to a polyvinylidene difluoride membrane. On the next day the membrane was blocked for 20 min with 5% bovine serum albumin (BSA) mixed with phosphate-buffered saline containing 0.05% tween-20 (PBS-T). The membrane was then incubated with primary antibodies against antiquitin and GAPDH overnight at 4^{O} C. Primary antibodies used were monoclonal anti-ALDH7A1 antibody (ab53278, Abcam) diluted 1:1000 in 5% BSA and PBS-T, and monoclonal anti-GAPDH antibody diluted 1:3000 in a similar buffer. The anti-ALDH7A1 antibody is directed against the C-terminal end of the protein. On the following day, the membrane was washed 2X for 15 min with PBS-T. The blot was then incubated with secondary antibodies (goat anti-rabbit, Alexa Fluor 680, Molecular Probes, Eugene, OR-or goat anti-mouse -IRDye 800, LI-COR) for 2 h at room temperature. Subsequently, the blot was washed 2X for 15 min with PBS-T. Finally, the blot was imaged and protein levels were quantified using a LI-COR Odyssey Infrared Imaging System.

Collection of samples for mass spectrometry analysis

For mass spectrometry analysis, mice were killed by decapitation. Brain and liver tissue samples were promptly harvested and snap-frozen with isopentane in dry ice. Blood was immediately collected from neck vessels in EDTA dipotassium tubes. The blood tubes were spun in a microcentrifuge at 3500–3600 rpm for 10 min to separate the plasma. The plasma was transferred to another tube and then quickly frozen with isopentane in dry ice. Tissue and plasma samples were stored in a -80^{O} C freezer until time of shipment to the analyzing laboratories.

Quantification of lysine metabolites

α-AASA and P6C in adult brain and liver were analyzed according to a published method (3) in methanol extracts prepared for amino acid analysis. Lysine, P6C, PIP, saccharopine and α-aminoadipic acid in brain and liver tissue from P0 mice were quantified using liquid chromatography–tandem mass spectrometry according to previously published methods (8, 18). Because P0 and adult samples were analyzed by different laboratories, the metabolites analyzed represent a non-overlapping set; namely, saccharopine was measured in P0 mice only (8) and AASA was measured in adult samples only (3).

Quantification of vitB6 vitamers

Pieces of snap-frozen liver and brain tissue were powdered in liquid nitrogen. Tissue powder was quickly weighed and 100 µL of ice cold trichloracetic acid (TCA; 50 g/l) per 10 mg tissue powder were added. The solutions were homogenized with zirconium oxide beads (0.5 mm) using a bullet blender tissue homogenizer (Next Advance Inc., Averill Park, NY, USA) for 5 min in stand 8 at 4°C following the manufacturers recommendations. The homogenates were centrifuged at 16 200 g for 5 min at 4°C. The supernatants were diluted 10 times with TCA (50 g/l) and 80 µL of the diluted sample was mixed with 80 µL of solution containing isotopically labeled internal standards, vortexed, incubated 15 min in the dark and centrifuged at 16 200 g for 5 min at 4°C. The supernatants were used for vitB6 vitamer analysis with UPLC–MS/MS as described in detail previously (51). The content of vitB6 vitamers was expressed in nmol per gram tissue wet

Table 1. Lysine and PN composition of modified diets in comparison with regular diet

Diet ID	Lysine level (%)	PN level (ppm)	Catalog no.
Special diet 1 (SD1)	4.7	1.6	TD.180908
Special diet 2 (SD2)	4.7	11.5	TD.180907
Regular diet	0.9	18	2018

weight. During all steps, samples were protected from light as much as possible.

Quantification of amino acids and methionine sulfoxide

Tissue powder was homogenized in methanol (100%; 100 µL per 10 mg tissue) using a bullet blender tissue homogenizer (Next Advance Inc., Averill Park, NY, USA) for 5 min in stand 8 at 4°C. The homogenates were centrifuged at 16 200 g for 5 min at 4°C. Amino acids and methionine sulfoxide were analyzed in undiluted supernatants using the UPLC–MS/MS as described previously (52). The content of amino acids was expressed in µmol per gram tissue wet weight. One WT sample was deemed an extreme outlier across multiple amino acids and was excluded from the final amino acid analyses due to suspicion of technical error.

Quantification of neurotransmitters

Gamma-aminobutyric acid (GABA) and glutamic acid were quantified in whole brain hemisphere and liver homogenates of P0 mice using liquid chromatography–tandem mass spectrometry according to previously published methods (18).

Biogenic amine neurotransmitters and their metabolites were analyzed in whole brain hemisphere homogenates (2% w/v homogenates in 0.08 M acetic acid) and plasma with liquid chromatography in combination with isotope dilution tandem mass spectrometry as previously described (53).

In vivo electrophysiology

In vivo EEG recordings were performed in WT and KO mice from two incipient congenic background strains: C57BL/6 J (B6/J) and 129 S1/SvImJ (129). Experiments included 3 KO and 3 WT mice of mixed sex (age: 10 months) from the B6/J strain and 2 KO and 2 WT mice (age: 2 months) from the 129 strain. The procedure consisted of three main steps: surgical implantation of electrodes, connection of the recording device, and data downloading and processing. All animal surgeries were carried out using aseptic techniques and in accordance with the guidelines of the Canadian Council on Animal Care and an approved protocol from the University of British Columbia Animal Care Committee (Animal Protocols # A14-0031 and A18-0117).

Electrode implantation surgery

For electrode placement, animals were anesthetized with 3% isoflurane and placed in a stereotaxic frame. After exposing the cranium, four burr holes were drilled bilaterally over the frontal and parietal cortices (approximate bregma coordinates were frontal: AP = +1.5 mm, ML = −/+1.8 mm, parietal: AP = −2.4 mm, ML = +/−2.2 mm) and one over the occipital segment (approximate bregma coordinates AP = −5.03, ML = +0.6). Miniature stainless-steel screws (Part No. 0–80 X 1/16, Invivo1, USA) presoldered to insulated copper wire leads were screwed into the skull holes with the above coordinates to serve as EEG electrodes. Four electrodes (the two frontal and two parietal) were used to record EEG signals. The bipolar occipital electrodes served as ground and reference electrodes. Wire terminals from these electrodes were connected to a 7-pin header mounted over the animal's head. The screws and the pin connector were further fixed in place by acrylic dental cement (Stoelting, USA). After surgery, mice were singly housed and allowed to recover for at least 3 weeks before proceeding with EEG recordings.

EEG recording

EEG recording was performed in freely moving animals using Neurologger 2A (Evolocus, USA, http://www.evolocus.com/neurologger-2A.htm). This wireless non-telemetric system allows EEG data to be stored directly on a memory chip that is integrated within the head mount unit. It is also equipped with a three-dimensional accelerometer that provides simultaneous tracking of animal movement during the EEG recording. To commence recording, Neurologger was connected to the implanted pin header with a pre-set sampling rate of 400 Hz. EEG was continuously recorded in each animal for 24–48 h.

Data acquisition and analysis

At the end of each recording session, Neurologger was disconnected from the animal's head and connected to a computer using a Neurologger USB Adapter (Evolocus, USA). EEG and accelerometer data were downloaded offline from the logger memory to a computer. Retrieved data were then converted from binary to text or Float32IE formats. Data downloading and conversion were carried out using the Downloader software tool version 1.27 (Evolocus, USA). Electrophysiological and accelerometer data were visualized and processed using EEGLAB versions 14.1.1 and 14.1.2 (Delorme and Makeig, 2004) running under Matlab version R2017b or R2019a (The MathWorks Inc., USA). Traces obtained from the four active EEG channels were plotted and analyzed in parallel with the synchronized animal acceleration data along the three orthogonal axes (x, y and z). EEG data were visually screened to identify potential convulsive seizure events. A convulsive seizure was defined by the presence of large-amplitude (>2x baseline), high-frequency (>5 Hz) discharges which were also associated with sudden and vigorous changes in the animal movement along the three accelerometer axes.

Behavioral testing

Two cohorts of mice were tested for behavioral abnormalities using a pipeline of neurobehavioral tests that consisted of open field, forced swim, novel object recognition, elevated plus maze, Morris water maze and accelerating rotarod tests. Cohort 1 was tested at an age of 6 months and included 16 WT and 13 KO mice of mixed sex. Cohort 2 was tested at an age of 2.5 months and consisted of 11 WT and 10 KO mice of mixed sex, except for accelerating rotarod test in which there were 9 WT and 8 KO mice. Mice used in behavioral tests were generated from HET intercrosses except for 3 WT mice in Cohort 1 and 2 WT mice in

Table 2. Summary of experiments performed in *Aldh7a1*-KO mice

Diet	Experiments performed (strain)	Age of mice	Number of mice	Compounds measured
Regular diet	Mass spectrometry analysis (B6/J)	10–22 weeks	8 KO, 8 HET, 8 WT	P6C, α-AASA, PIP, vitB6 vitamers, neurotransmitters, amino acids
		P0	5 KO, 5 HET, 5 WT[a]	P6C, PIP, SAC, α-AAA, lysine, vitB6 vitamers, GABA, glutamic acid
	in vivo EEG (B6/J and 129)	10 months (B6/J) 2 months (129)	3 KO, 3 WT 2 KO, 2 WT	
	Behavioral testing (B6/J)	6 months 2.5 months	13 KO, 16 WT 10 KO, 11 WT	
	Neuropathology (B6/J)	4 months	3 KO, 3 WT	
Special diets (SD1/SD2)	Seizure and survival analyses (B6/J and 129)	11–14.5 months (B6/J)	5 KO (untreated), 7 KO (treated), 12 WT	
		3 months (129)	1 KO (untreated), 1 KO (treated), 2 WT	
	Mass spectrometry analysis (B6/J)	11–14.5 months	4 KO (untreated), 5 KO (treated), 6 WT	PLP

[a]Except for vitB6 vitamers, where N = 3 per genotype. Abbreviations: P6C: Δ^1-piperideine-6-carboxylic acid; α-AASA: α-aminoadipic semialdehyde; PIP: pipecolic acid; SAC: saccharopine; α-AAA: α-aminoadipic acid; PLP: Pyridoxal 5′-phoshpate; GABA: Gamma-aminobutyric acid.

Cohort 2 which were generated from HET x WT crossings. Video analysis was carried out using EthoVision XT software versions 7.0 or 13.0 (Noldus, VA).

All behavioral tests were carried out as previously described (54) with the exception of small modifications to the protocol for the Morris water maze (MWM). The MWM test consisted of habituation to the pool on Day 1 followed by training to find a hidden platform on Days 2, 3 and 4. The probe trial was conducted on Day 8 (as opposed to Day 5 in previously published methods). For Cohort 2, an additional small modification was made in that an extra day of training was included on Day 5. This was done as the latency to find the hidden platform during training of WT mice in Cohort 1 was longer than expected and it was hypothesized that an extra day of training would improve overall performance. No significant difference was observed in latency to find the hidden platform whether the mice were given three or four training days. Data were analyzed separately and combined for the MWM and no significant differences were observed with any analysis. Thus, Cohorts 1 and 2 MWM performance data were analyzed separately for the final analysis.

Immunohistochemistry and neuropathological analysis

Mice were examined for neuropathological abnormalities by immunohistochemical techniques using two biomarkers; NeuN (marker for neurons) and GFAP (marker for astrocytes). Analysis was done on brain tissue sections obtained from 3 KO and 3 WT mice at 4 months of age. Brains were prepared for immunohistochemical staining and analysis as previously described (55). Antibodies used were as follows: the neuronal marker NeuN (Chemicon, Millipore, 1:2000, mouse monoclonal) and the astrocyte marker GFAP (Sigma; 1:2000, mouse monoclonal), and appropriate biotinylated secondary antibodies (Vector, 1:2000). On sections stained with GFAP, cresyl violet was used as a counterstain according to previously published methods (54).

An evaluation of gross brain structure, neuronal organization, and astrocytosis was performed as a qualitative assessment by two independent researchers. NeuN-stained slides were examined for neuron distribution and thickness of cortical layers, thickness of the corpus callosum, and general distribution and number of neurons in multiple additional brain structures (hippocampus, striatum, thalamus, cerebellum). GFAP slides were examined for the degree of immunoreactivity in the brain regions listed above.

Dietary modifications

To validate the effect of dietary lysine and PN in inducing a clinical phenotype in KO mice, we designed two types of special diets that vary in their lysine and/or PN contents (Table 1). Special Diet 1 (SD1) contained high lysine and minimal PN levels (in adult mice, PN at 1 ppm in diet is adequate for growth and maintenance [National Research Council, 1995]). SD1 was intended to induce an epileptic phenotype in KO mice. Special Diet 2 (SD2) contained high lysine and higher PN levels and was used along with PN injections to test the effect of PN in suppressing seizures induced by high lysine. All special diets were manufactured by Envigo (USA). Special diets were tested on mice in two stages; a pilot trial with small number of animals and then a follow-up trial with a larger cohort of mice.

Pilot dietary induction trial

All mice were originally fed the regular diet and underwent surgical EEG implantation and baseline EEG recording (described above) before being switched to special diets followed by post-diet EEG recording. In the pilot trial, mice were divided into two groups. The first group received SD1 without any treatment. The second group fed SD2 and the KOs further received daily PN-HCl injections i.p. at a dose of 200 μg/g of body weight starting from Day 2, which was reduced to 100 μg/g on Day 6 of the trial. Each group comprised 2 KO and 2 WT mice, one from each background strain. The age of the animals was 12 months for the B6/J mice and 3 months for the 129 mice. Mice were monitored and their diet consumption was recorded daily. Continuous EEG was collected for 24–36 h from each mouse

throughout the trial. The pilot experiment was terminated on Day 8.

Follow-up dietary induction experiments

In follow-up trials, mice were also divided to two dietary groups. The first group received SD1 without treatment and included 4 KO and 10 WT mice. The second group received SD2 and given i.p. injections of 200 µg/g PN-HCl q.o.d starting from Day 2. This group included 6 KO mice. Mice were checked on a daily basis and their body weights and diet consumption were recorded. Assessment of seizures in KO mice under SD1 was based on visual inspection; type, severity and duration of seizure events were recorded in monitoring sheets and also captured with by video recording. Seizing mice reaching a humane endpoint of seizure severity and frequency were euthanized according to approved criteria. Seizure severity was graded from 0–6 as follows: 0 = no visible signs of seizure, 1 = strong-pitched vocalizations, 2 = continuous running in the cage, 3 = tongue biting, 4 = twisting of trunk, ataxic gait, 5 = loss of consciousness in supine position, tonic–clonic extensions, tremors of the limbs, 6 = status epilepticus (SE): any of the above signs sustained for more than 3 min. The seizure scoring system was adapted from our previously published methods (56), with some modifications to reflect the seizure types that were anticipated in KO mice. Based on seizure severity (SS) and frequency, humane endpoints were defined as: SS = 1, 2, 3, 4 at frequency > 3/h or > 5/day, SS = 5 at frequency > 2/h or > 4/day, SS = 6 at frequency > 1/h or > 2/day; seizure causes self-inflicted trauma; or the animal becomes cyanotic or apneic during an attack. All mice used in follow-up trials were non-implanted, only from the B6/J strain and aged 11–14.5 months. All mice were followed up until Day 10 of the experiment, at which time the mice were sacrificed by CO_2 inhalation and the brain and liver tissue dissected and snap-frozen for future biochemical analysis. Assessment of PLP levels in these tissues was performed as described above (Quantification of vitB6 vitamers).

Table 2 summarizes the phenotyping experiments performed in mice under the regular and special diets along with number of mice and age timepoints for each experiment.

Statistical analysis

One-way ANOVA followed by *post-hoc* Dunnett's multiple comparisons test to correct for comparisons between multiple genotypes was used to compare mean concentrations in lysine metabolites, vitB6 vitamers, amino acids and methionine sulfoxide. Unpaired Student's *t*-test was used to compare mean concentrations in neurotransmitters. Lysine metabolite levels in the adult brain (P6C, AASA, PIP and SAC) constituted the primary outcome measures of the study. No multiple comparison correction to account for analysis of multiple additional compounds (7 vitB6 vitamers, 22 amino acids, methionine sulphoxide and 12 neurotransmitters) was performed; results for these analytes are shown with an uncorrected *P*-value and considered exploratory only. For analysis of correlation, Pearson correlation coefficient (Pearson's *r*) was used. Pearson's chi-squared ($\chi 2$) test was applied to test the Mendelian segregation of mice from heterozygous parents. Survival under modified diets was analyzed using the Kaplan–Meier method and the statistical difference between the curves was tested using the Log-rank (Mantel-Cox) test. All statistical analyses and graphical plotting of data were carried out using GraphPad Prism software. A *P*-value below 0.05 was considered significant.

Supplementary Data

Supplementary data mentioned in the text are available to subscribers in *HMG* online.

Acknowledgements

The authors would like to acknowledge the support of the Mouse Animal Production Service at the Centre of Molecular Medicine and Therapeutics at The University of British Columbia. This project was funded by research grants from The Rare Diseases: Models & Mechanisms Network (grant # 27R21814), The Canadian Institutes of Health Research (CIHR) and British Columbia Children's Hospital Research Institute (Brain, Behaviour & Development and Evidence to Innovation Research Themes). H.H.A.S. is supported by doctoral scholarship from the Ministry of Higher Education, Oman, and Al Awael Overseas Company LLC, Oman.

Conflict of Interest Statement. The authors declare no conflict of interest.

References

1. Coughlin, C.R., 2nd, Swanson, M.A., Spector, E., Meeks, N.J.L., Kronquist, K.E., Aslamy, M., Wempe, M.F., van Karnebeek, C.D.M., Gospe, S.M., Jr., Aziz, V.G. *et al.* (2019) The genotypic spectrum of ALDH7A1 mutations resulting in pyridoxine dependent epilepsy: a common epileptic encephalopathy. *J. Inherit. Metab. Dis.*, **42**, 353–361.
2. Stockler, S., Plecko, B., Gospe, S.M., Jr., Coulter-Mackie, M., Connolly, M., van Karnebeek, C., Mercimek-Mahmutoglu, S., Hartmann, H., Scharer, G., Struijs, E. *et al.* (2011) Pyridoxine dependent epilepsy and antiquitin deficiency: clinical and molecular characteristics and recommendations for diagnosis, treatment and follow-up. *Mol. Genet. Metab.*, **104**, 48–60.
3. Mills, P.B., Struys, E., Jakobs, C., Plecko, B., Baxter, P., Baumgartner, M., Willemsen, M.A., Omran, H., Tacke, U., Uhlenberg, B. *et al.* (2006) Mutations in antiquitin in individuals with pyridoxine-dependent seizures. *Nat. Med.*, **12**, 307–309.
4. van Karnebeek, C.D., Tiebout, S.A., Niermeijer, J., Poll-The, B.T., Ghani, A., Coughlin, C.R., 2nd, Van Hove, J.L., Richter, J.W., Christen, H.J., Gallagher, R. *et al.* (2016) Pyridoxine-dependent epilepsy: an expanding clinical Spectrum. *Pediatr. Neurol.*, **59**, 6–12.
5. Mills, P.B., Footitt, E.J., Mills, K.A., Tuschl, K., Aylett, S., Varadkar, S., Hemingway, C., Marlow, N., Rennie, J., Baxter, P. *et al.* (2010) Genotypic and phenotypic spectrum of pyridoxine-dependent epilepsy (ALDH7A1 deficiency). *Brain*, **133**, 2148–2159.
6. Yusuf, I.H., Sandford, V. and Hildebrand, G.D. (2013) Congenital cataract in a child with pyridoxine-dependent epilepsy. *J. AAPOS*, **17**, 315–317.
7. van Karnebeek, C.D., Stockler-Ipsiroglu, S., Jaggumantri, S., Assmann, B., Baxter, P., Buhas, D., Bok, L.A., Cheng, B., Coughlin, C.R., 2nd, Das, A.M. *et al.* (2014) Lysine-restricted diet as adjunct therapy for pyridoxine-dependent epilepsy: the PDE consortium consensus recommendations. *JIMD Rep.*, **15**, 1–11.
8. Pena, I.A., Marques, L.A., Laranjeira Â, B., Yunes, J.A., Eberlin, M.N., MacKenzie, A. and Arruda, P. (2017) Mouse lysine

catabolism to aminoadipate occurs primarily through the saccharopine pathway; implications for pyridoxine dependent epilepsy (PDE). *Biochim. Biophys. Acta Mol. Basis Dis.*, **1863**, 121–128.
9. Coughlin, C.R., 2nd, van Karnebeek, C.D., Al-Hertani, W., Shuen, A.Y., Jaggumantri, S., Jack, R.M., Gaughan, S., Burns, C., Mirsky, D.M., Gallagher, R.C. *et al.* (2015) Triple therapy with pyridoxine, arginine supplementation and dietary lysine restriction in pyridoxine-dependent epilepsy: neurodevelopmental outcome. *Mol. Genet. Metab.*, **116**, 35–43.
10. Mahajnah, M., Corderio, D., Austin, V., Herd, S., Mutch, C., Carter, M., Struys, E. and Mercimek-Mahmutoglu, S. (2016) A prospective case study of the safety and efficacy of lysine-restricted diet and arginine supplementation therapy in a patient with pyridoxine-dependent epilepsy caused by mutations in ALDH7A1. *Pediatr. Neurol.*, **60**, 60–65.
11. Mercimek-Mahmutoglu, S., Corderio, D., Nagy, L., Mutch, C., Carter, M., Struys, E. and Kyriakopoulou, L. (2014) Lysine-restricted diet and mild cerebral serotonin deficiency in a patient with pyridoxine-dependent epilepsy caused by ALDH7A1 genetic defect. *Mol. Genet. Metab. Rep.*, **1**, 124–128.
12. Jansen, L.A., Hevner, R.F., Roden, W.H., Hahn, S.H., Jung, S. and Gospe, S.M., Jr. (2014) Glial localization of antiquitin: implications for pyridoxine-dependent epilepsy. *Ann. Neurol.*, **75**, 22–32.
13. Struys, E.A., Bok, L.A., Emal, D., Houterman, S., Willemsen, M.A. and Jakobs, C. (2012) The measurement of urinary Delta(1)-piperideine-6-carboxylate, the alter ego of alpha-aminoadipic semialdehyde, in Antiquitin deficiency. *J. Inherit. Metab. Dis.*, **35**, 909–916.
14. Engstrom, F.L. and Woodbury, D.M. (1988) Seizure susceptibility in DBA and C57 mice: the effects of various convulsants. *Epilepsia*, **29**, 389–395.
15. Ferraro, T.N., Golden, G.T., Smith, G.G. and Berrettini, W.H. (1995) Differential susceptibility to seizures induced by systemic kainic acid treatment in mature DBA/2J and C57BL/6J mice. *Epilepsia*, **36**, 301–307.
16. Ferraro, T.N., Golden, G.T., Smith, G.G., DeMuth, D., Buono, R.J. and Berrettini, W.H. (2002) Mouse strain variation in maximal electroshock seizure threshold. *Brain Res.*, **936**, 82–86.
17. Kosobud, A.E. and Crabbe, J.C. (1990) Genetic correlations among inbred strain sensitivities to convulsions induced by 9 convulsant drugs. *Brain Res.*, **526**, 8–16.
18. Pena, I.A., Roussel, Y., Daniel, K., Mongeon, K., Johnstone, D., Weinschutz Mendes, H., Bosma, M., Saxena, V., Lepage, N., Chakraborty, P. *et al.* (2017) Pyridoxine-dependent epilepsy in Zebrafish caused by Aldh7a1 deficiency. *Genetics*, **207**, 1501–1518.
19. Crowther, L.M., Mathis, D., Poms, M. and Plecko, B. (2019) New insights into human lysine degradation pathways with relevance to pyridoxine-dependent epilepsy due to antiquitin deficiency. *J. Inherit. Metab. Dis.*, **42**, 620–628.
20. Wempe, M.F., Kumar, A., Kumar, V., Choi, Y.J., Swanson, M.A., Friederich, M.W., Hyland, K., Yue, W.W., Van Hove, J.L.K. and 2nd Coughlin, C.R. (2019) Identification of a novel biomarker for pyridoxine-dependent epilepsy: implications for newborn screening. *J. Inherit. Metab. Dis.*, **42**, 565–574.
21. Posset, R., Opp, S., Struys, E.A., Völkl, A., Mohr, H., Hoffmann, G.F., Kölker, S., Sauer, S.W. and Okun, J.G. (2015) Understanding cerebral L-lysine metabolism: the role of L-pipecolate metabolism in Gcdh-deficient mice as a model for glutaric aciduria type I. *J. Inherit. Metab. Dis.*, **38**, 265–272.
22. Struys, E.A. and Jakobs, C. (2010) Metabolism of lysine in alpha-aminoadipic semialdehyde dehydrogenase-deficient fibroblasts: evidence for an alternative pathway of pipecolic acid formation. *FEBS Lett.*, **584**, 181–186.
23. Struys, E.A., Jansen, E.E. and Salomons, G.S. (2014) Human pyrroline-5-carboxylate reductase (PYCR1) acts on $\Delta(1)$-piperideine-6-carboxylate generating L-pipecolic acid. *J. Inherit. Metab. Dis.*, **37**, 327–332.
24. Mercimek-Mahmutoglu, S., Cordeiro, D., Cruz, V., Hyland, K., Struys, E.A., Kyriakopoulou, L. and Mamak, E. (2014) Novel therapy for pyridoxine dependent epilepsy due to ALDH7A1 genetic defect: L-arginine supplementation alternative to lysine-restricted diet. *Eur. J. Paediatr. Neurol.*, **18**, 741–746.
25. Biagosch, C., Ediga, R.D., Hensler, S.V., Faerberboeck, M., Kuehn, R., Wurst, W., Meitinger, T., Kölker, S., Sauer, S. and Prokisch, H. (2017) Elevated glutaric acid levels in Dhtkd1−/Gcdh- double knockout mice challenge our current understanding of lysine metabolism. *Biochim. Biophys. Acta Mol. Basis Dis.*, **1863**, 2220–2228.
26. Hallen, A., Jamie, J.F. and Cooper, A.J. (2013) Lysine metabolism in mammalian brain: an update on the importance of recent discoveries. *Amino Acids*, **45**, 1249–1272.
27. Murthy, S.N. and Janardanasarma, M.K. (1999) Identification of L-amino acid/L-lysine alpha-amino oxidase in mouse brain. *Mol. Cell. Biochem.*, **197**, 13–23.
28. Sauer, S.W., Opp, S., Hoffmann, G.F., Koeller, D.M., Okun, J.G. and Kolker, S. (2011) Therapeutic modulation of cerebral L-lysine metabolism in a mouse model for glutaric aciduria type I. *Brain*, **134**, 157–170.
29. Kim, J.S. and Giacobini, E. (1985) Pipecolic acid levels and transport in developing mouse brain. *Brain Res.*, **354**, 181–186.
30. Rao, V.V., Tsai, M.J., Pan, X. and Chang, Y.F. (1993) L-pipecolic acid oxidation in rat: subcellular localization and developmental study. *Biochim. Biophys. Acta*, **1164**, 29–35.
31. Hoffmann, G.F., Schmitt, B., Windfuhr, M., Wagner, N., Strehl, H., Bagci, S., Franz, A.R., Mills, P.B., Clayton, P.T., Baumgartner, M.R. *et al.* (2007) Pyridoxal 5′-phosphate may be curative in early-onset epileptic encephalopathy. *J. Inherit. Metab. Dis.*, **30**, 96–99.
32. Ramos, R.J., Pras-Raves, M.L., Gerrits, J., van der Ham, M., Willemsen, M., Prinsen, H., Burgering, B., Jans, J.J. and Verhoeven-Duif, N.M. (2017) Vitamin B6 is essential for serine de novo biosynthesis. *J. Inherit. Metab. Dis.*, **40**, 883–891.
33. Paulose, C.S., Dakshinamurti, K., Packer, S. and Stephens, N.L. (1988) Sympathetic stimulation and hypertension in the pyridoxine-deficient adult rat. *Hypertension (Dallas, Tex. : 1979)*, (11), 387–391.
34. Brocker, C., Cantore, M., Failli, P. and Vasiliou, V. (2011) Aldehyde dehydrogenase 7A1 (ALDH7A1) attenuates reactive aldehyde and oxidative stress induced cytotoxicity. *Chem. Biol. Interact.*, **191**, 269–277.
35. Mashima, R., Nakanishi-Ueda, T. and Yamamoto, Y. (2003) Simultaneous determination of methionine sulfoxide and methionine in blood plasma using gas chromatography-mass spectrometry. *Anal. Biochem.*, **313**, 28–33.
36. Suzuki, S., Kodera, Y., Saito, T., Fujimoto, K., Momozono, A., Hayashi, A., Kamata, Y. and Shichiri, M. (2016) Methionine sulfoxides in serum proteins as potential clinical biomarkers of oxidative stress. *Sci. Rep.*, **6**, 38299.
37. Brown, D.R. and Kretzschmar, H.A. (1998) The glio-toxic mechanism of alpha-aminoadipic acid on cultured astrocytes. *J. Neurocytol.*, **27**, 109–118.
38. Huck, S., Grass, F. and Hörtnagl, H. (1984) The glutamate analogue alpha-aminoadipic acid is taken up by astrocytes before exerting its gliotoxic effect in vitro. *J. Neurosci.*, **4**, 2650–2657.

39. Khurgel, M., Koo, A.C. and Ivy, G.O. (1996) Selective ablation of astrocytes by intracerebral injections of alpha-aminoadipate. *Glia*, **16**, 351–358.
40. Zhou, J., Wang, X., Wang, M., Chang, Y., Zhang, F., Ban, Z., Tang, R., Gan, Q., Wu, S., Guo, Y. *et al.* (2019) The lysine catabolite saccharopine impairs development by disrupting mitochondrial homeostasis. *J. Cell Biol.*, **218**, 580–597.
41. Naasan, G., Yabroudi, M., Rahi, A. and Mikati, M.A. (2009) Electroencephalographic changes in pyridoxine-dependant epilepsy: new observations. *Epileptic Disord.*, **11**, 293–300.
42. Nabbout, R., Soufflet, C., Plouin, P. and Dulac, O. (1999) Pyridoxine dependent epilepsy: a suggestive electroclinical pattern. *Arch. Dis. Child. Fetal Neonatal Ed.*, **81**, F125–F129.
43. Gallagher, R.C., Van Hove, J.L., Scharer, G., Hyland, K., Plecko, B., Waters, P.J., Mercimek-Mahmutoglu, S., Stockler-Ipsiroglu, S., Salomons, G.S., Rosenberg, E.H. *et al.* (2009) Folinic acid-responsive seizures are identical to pyridoxine-dependent epilepsy. *Ann. Neurol.*, **65**, 550–556.
44. Millet, A., Salomons, G.S., Cneude, F., Corne, C., Debillon, T., Jakobs, C., Struys, E. and Hamelin, S. (2011) Novel mutations in pyridoxine-dependent epilepsy. *Eur. J. Paediatr. Neurol.*, **15**, 74–77.
45. Yeghiazaryan, N.S., Striano, P., Spaccini, L., Pezzella, M., Cassandrini, D., Zara, F. and Mastrangelo, M. (2011) Long-term follow-up in two siblings with pyridoxine-dependent seizures associated with a novel ALDH7A1 mutation. *Eur. J. Paediatr. Neurol.*, **15**, 547–550.
46. Mouse., N.R.C.U.S.o.L.A.N.N.R.o.t. (1995) *Nutrient Requirements of Laboratory Animals*: 4th revised edn. Available from: https://www.ncbi.nlm.nih.gov/books/NBK231918/.
47. Mathis, D., Abela, L., Albersen, M., Bürer, C., Crowther, L., Beese, K., Hartmann, H., Bok, L.A., Struys, E., Papuc, S.M. *et al.* (2016) The value of plasma vitamin B6 profiles in early onset epileptic encephalopathies. *J. Inherit. Metab. Dis.*, **39**, 733–741.
48. Pérez, B., Gutiérrez-Solana, L.G., Verdú, A., Merinero, B., Yuste-Checa, P., Ruiz-Sala, P., Calvo, R., Jalan, A., Marín, L.L., Campos, O. *et al.* (2013) Clinical, biochemical, and molecular studies in pyridoxine-dependent epilepsy. Antisense therapy as possible new therapeutic option. *Epilepsia*, **54**, 239–248.
49. Ebino, K.Y. (1993) Studies on coprophagy in experimental animals. *Jikken Dobutsu. Exp. Anim.*, **42**, 1–9.
50. Pettitt, S.J., Liang, Q., Rairdan, X.Y., Moran, J.L., Prosser, H.M., Beier, D.R., Lloyd, K.C., Bradley, A. and Skarnes, W.C. (2009) Agouti C57BL/6N embryonic stem cells for mouse genetic resources. *Nat. Methods*, **6**, 493–495.
51. van der Ham, M., Albersen, M., de Koning, T.J., Visser, G., Middendorp, A., Bosma, M., Verhoeven-Duif, N.M. and de Sain-van der Velden, M.G. (2012) Quantification of vitamin B6 vitamers in human cerebrospinal fluid by ultra performance liquid chromatography-tandem mass spectrometry. *Anal. Chim. Acta*, **712**, 108–114.
52. Prinsen, H., Schiebergen-Bronkhorst, B.G.M., Roeleveld, M.W., Jans, J.J.M., de Sain-van der Velden, M.G.M., Visser, G., van Hasselt, P.M. and Verhoeven-Duif, N.M. (2016) Rapid quantification of underivatized amino acids in plasma by hydrophilic interaction liquid chromatography (HILIC) coupled with tandem mass-spectrometry. *J. Inherit. Metab. Dis.*, **39**, 651–660.
53. van Vliet, D., Bruinenberg, V.M., Mazzola, P.N., van Faassen, M.H., de Blaauw, P., Kema, I.P., Heiner-Fokkema, M.R., van Anholt, R.D., van der Zee, E.A. and van Spronsen, F.J. (2015) Large neutral amino acid supplementation exerts its effect through three synergistic mechanisms: proof of principle in phenylketonuria mice. *PLoS One*, **10**, e0143833.
54. Petkau, T.L., Neal, S.J., Milnerwood, A., Mew, A., Hill, A.M., Orban, P., Gregg, J., Lu, G., Feldman, H.H., Mackenzie, I.R. *et al.* (2012) Synaptic dysfunction in progranulin-deficient mice. *Neurobiol. Dis.*, **45**, 711–722.
55. Petkau, T.L., Hill, A., Connolly, C., Lu, G., Wagner, P., Kosior, N., Blanco, J. and Leavitt, B.R. (2019) Mutant huntingtin expression in microglia is neither required nor sufficient to cause the Huntington's disease-like phenotype in BACHD mice. *Hum. Mol. Genet.*, **28**, 1661–1670.
56. Petkau, T.L., Zhu, S., Lu, G., Fernando, S., Cynader, M. and Leavitt, B.R. (2013) Sensitivity to neurotoxic stress is not increased in progranulin-deficient mice. *Neurobiol. Aging*, **34**, 2548–2550.